Monthly Notices
of the
ROYAL ASTRONOMICAL SOCIETY

MNRAS **437,** 3603–3625 (2014)
Advance Access publication 2013 December 10

doi:10.1093/mnras/stt2156

A 1500 deg^2 near infrared proper motion catalogue from the UKIDSS Large Area Survey

Leigh Smith,[1⋆] P. W. Lucas,[1] B. Burningham,[1] H. R. A. Jones,[1] R. L. Smart,[2] A. H. Andrei,[1,3,4] S. Catalán[5] and D. J. Pinfield[1]

[1] *Centre for Astrophysics Research, Science and Technology Research Institute, University of Hertfordshire, Hatfield AL10 9AB, UK*
[2] *Istituto Nazionale di Astrofisica, Osservatorio Astrofisico di Torino, Strada Osservatorio 20, I-10025 Pino Torinese, Italy*
[3] *Observatório Nacional/MCTI, R. General José Cristino 77, CEP 20921-400 Rio de Janeiro – RJ, Brazil*
[4] *Observatório do Valongo/UFRJ, Ladeira do Pedro Antônio 43, CEP 20080-090 Rio de Janeiro – RJ, Brazil*
[5] *Department of Physics, University of Warwick, Coventry CV4 7AL, UK*

Accepted 2013 November 5. Received 2013 November 4; in original form 2013 September 9

ABSTRACT

The United Kingdom Infrared Deep Sky Survey (UKIDSS) Large Area Survey (LAS) began in 2005, with the start of the UKIDSS programme as a 7 year effort to survey roughly 4000 deg^2 at high Galactic latitudes in *Y, J, H* and *K* bands. The survey also included a significant quantity of two epoch *J* band observations, with an epoch baseline greater than 2 years to calculate proper motions. We present a near-infrared proper motion catalogue for the 1500 deg^2 of the two epoch LAS data, which includes 135 625 stellar sources and a further 88 324 with ambiguous morphological classifications, all with motions detected above the 5σ level. We developed a custom proper motion pipeline which we describe here. Our catalogue agrees well with the proper motion data supplied for a 300 deg^2 subset in the current Wide Field Camera Science Archive (WSA) 10th data release (DR10) catalogue, and in various optical catalogues, but it benefits from a larger matching radius and hence a larger upper proper motion detection limit. We provide absolute proper motions, using LAS galaxies for the relative to absolute correction. By using local second-order polynomial transformations, as opposed to linear transformations in the WSA, we correct better for any local distortions in the focal plane, not including the radial distortion that is removed by the UKIDSS pipeline. We present the results of proper motion searches for new brown dwarfs and white dwarfs. We discuss 41 sources in the WSA DR10 overlap with our catalogue with proper motions >300 mas yr^{-1}, several of which are new detections. We present 15 new candidate ultracool dwarf binary systems.

Key words: catalogues – proper motions – binaries: general – brown dwarfs – stars: kinematics and dynamics – stars: low-mass.

1 INTRODUCTION

Stellar proper motion is the apparent angular movement of a star in a given time period. All stars have some component of motion (depending on the reference frame) due to their motion around the Galaxy and 'gravitational kicks' they receive through interaction with other massive objects, usually molecular or atomic clouds. Motion perpendicular to a line between the star and the observer is the proper motion, which can be measured through careful observation of its position over two or more epochs, given sufficient time between observations dependent on instrument precision. Given its relationship with distance and tangential velocity ($V_{\rm tan} \propto d \cdot \mu$), a large proper motion is indicative of a fast moving and/or nearby source. For this reason, many of the stars in the solar neighbourhood were first identified due to their large proper motion.

Major proper motion catalogues of the last half of the 20th century were developed using large-scale surveys of Schmidt photographic plates often separated in time by many decades. Large-scale, deep, infrared sky surveys are very much a new thing as the size of infrared imaging arrays did not, until recently, permit them. The Two Micron All Sky Survey (2MASS; Skrutskie et al. 2006) and the Deep Near Infrared Survey of the Southern Sky (DENIS; Epchtein et al. 1997) are early examples of such surveys capitalizing on recent improvements in infrared array technology. 2MASS and DENIS utilized 256 × 256 pixel mercury cadmium telluride arrays. 2MASS used a pair of automated 1.3 m telescopes, one in each hemisphere, and DENIS used a single 1 m telescope at La Silla observatory in Chile. Some proper motion catalogues have used near-infrared data in conjunction with older optical catalogues to provide large

⋆ E-mail: l.smith10@herts.ac.uk

epoch baselines, which improve the precision of the proper motion measurement, and also include accurate near-infrared photometry (e.g. PPMXL; Roeser, Demleitner & Schilbach 2010 and SIPS; Deacon, Hambly & Cooke 2005). However, for a proper motion to be measured it must be detected in both surveys, meaning that very red objects which were not detected in the optical survey are missed. To overcome the problem of poor detectability of very red objects in such proper motion catalogues it is necessary to use infrared sky surveys alone. If we consider the use of 2MASS as the first epoch in a hypothetical near-infrared only proper motion catalogue, then the current maximum epoch baseline of such a survey is 15 years. The astrometric accuracy of near-infrared arrays is generally better than that of the Schmidt plates, which helps to offset the reduction in proper motion measurement precision due to shorter epoch baselines. Examples of current near-infrared only proper motion surveys include a 2MASS only proper motion search (Kirkpatrick et al. 2010) and a 2MASS United Kingdom Infrared Telescope (UKIRT) Infrared Deep Sky Survey (UKIDSS) based proper motion search (Deacon et al. 2009). Kirkpatrick et al. (2010) identified 107 proper motion candidates that lack counterparts in Digitized Sky Survey *B*, *R* and *I* band images. Both examples have also identified a multitude of new nearby red objects (ultracool dwarfs, UCDs), very few of which are detectable in current optical based surveys.

Proper motion information is particularly useful when attempting to identify members of gravitationally bound systems. Their members serve as useful benchmark objects when one or more components of their systems have measurable attributes (e.g. age and metallicity). Since members of such systems can be assumed to have formed from the same molecular cloud at a similar time, these attributes can also be inferred to belong to all members of a system (Pinfield et al. 2006). This is particularly useful in cases where it is difficult to constrain these attributes observationally, when dealing with UCDs for example. Well-characterized main-sequence stars and white dwarfs make good companions for benchmark systems. Identification of a common proper motion and common distance is usually required to link multiple stars as single, gravitationally bound systems.

UCDs, generally regarded as spectral type M7 or later, are very low mass stars and brown dwarfs. They are chemically very interesting since their cool atmospheres allow dust and molecules to form. A census of UCDs is necessary to constrain the mass function at the substellar end, filling in the gap between giant planets and low-mass stars (Burgasser 2004; Pinfield et al. 2006; Kirkpatrick 2011). UCDs are usually selected photometrically in the infrared, often combined with optical photometry (Pinfield et al. 2008; Burningham et al. 2010; Burgasser et al. 2011; Day-Jones et al. 2011; Deacon et al. 2012), though spectroscopic confirmation is still necessary (Pinfield et al. 2008; Day-Jones et al. 2011; Kirkpatrick et al. 2011). Proper motion is useful to discriminate between nearby UCDs and background objects with similar colours such as high-redshift quasars and giant stars (Looper, Kirkpatrick & Burgasser 2007; Sheppard & Cushing 2009; Deacon et al. 2012).

There are currently very few deep, wide field, near-infrared proper motion surveys. This paper presents a new catalogue, which can be expected to reveal objects not detected in optical surveys while also providing kinematic data for known objects that can serve many scientific purposes, such as investigating the ages of T dwarfs (Smith et al. 2013).

This paper is organized as follows. In Section 2, we describe the available data. In Section 3, we describe our pipeline and construction of the catalogue which is available in the online data. A sample of the catalogue is available in the appendix of this paper. In Section 4, we determine the accuracy and reliability of the catalogue and discuss known limitations. In Section 5, we outline searches undertaken for objects of interest within the catalogue. In Section 6, we reveal interesting sources identified during searches for multiple systems. In Section 7, we draw conclusions.

2 DATA

The UKIDSS (Warren 2002; Lawrence et al. 2007) project began in 2005, and was a 7 year effort to survey approximately 7000 deg^2 using the 3.8 m infrared-dedicated UKIRT, situated at the summit of Mauna Kea, Hawaii and the Wide Field CAMera (WFCAM; Casali et al. 2001, 2007).

The WFCAM consists of four 2048 × 2048 pixel arrays, which combined with UKIRT optics give a total viewing area of 0.21 deg^2 (0.4 arcsec per pixel; Casali et al. 2007). During observation, the arrays were microstepped for the UKIDSS Large Area Survey (ULAS) *J* band, four individual exposures are taken, each with a 0.5 pixel offset in *x* and/or *y* from the first and recombined during the Cambridge Astronomy Survey Unit (CASU) pipeline using a process called interleaving (Vick et al. 2004). Interleaving is performed using a process called *dribbling*, which corrects point spread function (PSF) mismatches caused by changes in the observing conditions between exposures, which can lead to a 'spiky' PSF.[1] This process of oversampling improves the resolution of the WFCAM images to the limit of the seeing. The WFCAM photometric system is described in detail in Hewett et al. (2006). After the CASU pipeline the data are then transferred to the WFCAM Science Archive (WSA; Hambly et al. 2008) for further processing and to make the data available for the community.

The Large Area Survey (LAS) covers 3800 deg^2 in *YJHK* passbands to an approximate 5σ depth of 19.6 in J and is complemented in the *ugriz* optical passbands by the Sloan Digital Sky Survey (SDSS). The LAS included a second epoch of observations in the J passband to calculate proper motions and investigate stellar variability. In the final months of the UKIDSS programme great effort was made to observe as much of the first epoch coverage as possible at second epoch. The final second epoch coverage is around 1500 deg^2.

UKIDSS LAS multiframe catalogues based on *J* band images taken during the period 2005 May 15 until 2012 May 20 were obtained from the WSA (Hambly et al. 2008) and paired using the telescope pointing coordinates to identify coincident multiframes. In many cases, several repeats of each pointing had been obtained over a relatively short period of time (typically days, weeks or months). This reflects the fact that multiframes may be rejected as part of the at-the-telescope survey quality control, and thus queued for repeats, but are still processed and committed to the archive. To ensure that the best quality frames were used for our first and second epochs at each pointing and avoid the use of deprecated frames, we only accepted pairs of multiframes where both multiframes represented the latest date amongst data taken at each epoch. This resulted in typical epoch baselines between multiframes of between 1.8 and 7 years.

We constructed two epoch catalogues for each pointing by matching sources within the pairs of multiframes using the Starlink Tables Infrastructure Library Tool Set (STILTS; Taylor 2006). We required

[1] CASU, http://casu.ast.cam.ac.uk/surveys-projects/wfcam/technical/interleaving

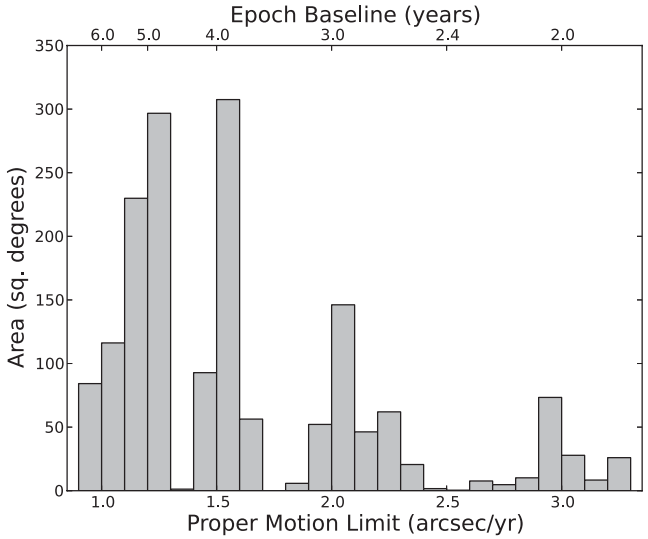

Figure 1. Plot showing the area distribution of epoch baselines and proper motion limits of the catalogue. Note that the total area represented by this plot is 1678 deg^2, this is simply the number of frames multiplied by the angular area of a frame, the catalogue is nearer to 1500 deg^2 after removal of the duplicated regions of frame overlaps.

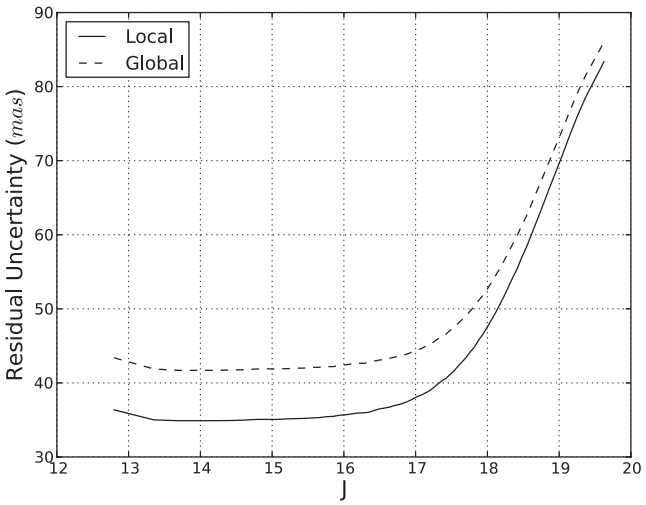

Figure 2. We selected sources meeting the criteria in Section 4.1 with measured local and global residuals (3.5 million sources total) and split them into 70 equal sized J magnitude bins. Note that the exact width in J magnitudes of each bin was allowed to be different, giving greater resolution where the source density allowed but maintaining accuracy at the extreme ends. The mean local and global residual uncertainties in each bin are shown. The local residual uncertainties are consistently lower than the global ones.

pairs of sources to be uniquely paired to their closest match within 6 arcsec, and we required the *J* band magnitudes for the two epochs to agree within 0.5 mag, to minimize mismatches. Given the minimum epoch baseline of 1.8 years, the hard proper motion limit of the catalogue is therefore 3.3 arcsec yr^{-1} though the catalogue is built from frame sets with a range of epoch baselines, giving a range of proper motion limits. Fig. 1 shows the area distribution of the epoch baselines and the corresponding proper motion limits. Note that we performed an initial rejection of the few input sources brighter than 12th or fainter than 20th magnitude in the *J* band (see Section 4.6).

3 METHOD

3.1 Overview

The method involves selecting a sample of good reference stars based on a variety of astrometric and photometric cuts. We then fit the motion between the two epochs using a second-order polynomial either locally or across the whole array, depending on the local source density and proximity to the edge of the array. Motions of most sources are calculated using a unique local fit to stars well distributed around them. We use local transformations in preference as they produce more accurate results (see Fig. 2).

3.2 Definitions

In this paper, we adopt the following terms, consistent with those used by the WSA.

Frame – an image or catalogue data from one of the four WFCAM arrays.

Frame set – a set of frames covering the same area and multiple bandpass and/or epochs.

Multiframe – a set of four frames comprising one whole WFCAM footprint in one bandpass and epoch (exclusive of the guider chip).

For the purpose of this description, we adopt the following terms.

Global (fit/transform) – the operation was performed using all relevant data in one frame.

Local (fit/transform) – the operation was performed using a limited area of one frame.

Target (source/frame) – where an operation is performed on each source/frame individually, we refer to an example as the *target* source/frame.

J1 and J2 – refer to the first and second epoch *J* band images, respectively.

3.3 Reference star selection

A preliminary pool of astrometric reference sources was created as a subset of the input catalogue, containing sources meeting the following criteria.

Classified as stellar at J1 and J2;
J1 and J2 between 16 and 19.6;
J1 and J2 magnitude error <0.1; and
J1 and J2 ellipticity <0.3.

We rejected frames containing fewer than 20 reference sources. The minimum requirement for a second-order polynomial fit is 6 but we adopted 20 to ensure the data were well fitted across the frame. In practice, we rejected 217 frame sets (0.65 per cent), losing 46 097 sources (0.26 per cent) at this stage.

On a frame-by-frame basis, we fit the second epoch array (*x*/*y*) positions of the reference sources to their first epoch array positions using a second-order polynomial fit and the CP2TFORM function in MATLAB to produce a preliminary global transform. We applied the inverse of this coordinate transformation (MATLAB does not allow a forward transformation for a second-order polynomial) to map the first epoch reference source positions on to the second epoch positions and subtracted these from their second epoch positions to produce preliminary residuals. We measured the uncertainty on the

preliminary residuals by calculating the rms residual to the fit of all reference sources in each frame and added these in quadrature to their centroid errors.

We rejected all reference stars with significant preliminary residuals ($>1\sigma$) usually indicating motion. We then discarded all preliminary positions and motions and performed a further rejection of frames failing the minimum 20 reference stars cut. A further 144 frame sets (42 415 sources) were rejected at this stage taking the frame and source counts to 33 038 and 17 122 488, respectively.

Note that we use array coordinates to calculate the motions since the astrometric fit of LAS frames is performed by CASU using the positions of 2MASS sources, which were observed near epoch 2000. The quality of these fits has degraded over time due to the motions of the 2MASS sources used.

3.4 Second epoch position correction

Final residuals are calculated on a source-by-source basis. We select all reference stars (with the exception of the target source) in the same frame as the target source as a temporary pool of reference stars. We calculate a global transform by fitting the first epoch reference star array positions to the second epoch reference star array positions using a second-order polynomial as before, and apply the inverse coordinate transformation to the second epoch target position to map them on to the first epoch array coordinate system. We then calculate the rms residual to the fit of the reference sources and add it in quadrature to the centroid error of the target at the second epoch to calculate the uncertainty on the transformed position.

Another second-order polynomial fit was then calculated and applied in the same manner but using only reference stars local to the target. We selected all reference stars within a radius sufficient to ensure that there were at least three in every attached circle quadrant. This radius was rounded up to the nearest 20 arcsec and we impose a minimum radius of 1 arcmin.

The use of this method ensured that there were at least 12 reference stars used to calculate each fit and crucially that the reference stars were well distributed about the target source. If any quadrant contained fewer than three reference stars then a local polynomial was not calculated and we default to using the global polynomial to calculate a final proper motion. This was always the case for sources at the edge of frames. A 'true' value in the local column of the catalogue indicates that a source has a proper motion calculated using a local transform. We applied the local polynomial to the target source's second epoch position to map it on to the first epoch array coordinate system. We then follow the same uncertainty calculation method as before.

To calculate proper motion, we used residuals calculated from the local transforms in preference to the global ones. We justify this preference by looking at the uncertainties on the total residuals for the two samples (see Fig. 2), where the local transform produces smaller average uncertainties on the residuals than the global transform.

3.5 Conversion to equatorial coordinate system

In order to transform the array coordinate positions on to the tangent plane to the equatorial system, the first epoch α/δ positions underwent a tangent plane projection conversion about the centre of the frame, producing ξ/η positions.

$$\xi = \frac{\cos\delta\sin(\alpha-\bar{\alpha})}{\sin\delta\sin\bar{\delta}+\cos\delta\cos\bar{\delta}\cos(\alpha-\bar{\alpha})} \tag{1a}$$

$$\eta = \frac{\sin\delta\cos\bar{\delta}-\cos\delta\sin\bar{\delta}\cos(\alpha-\bar{\alpha})}{\sin\delta\sin\bar{\delta}+\cos\delta\cos\bar{\delta}\cos(\alpha-\bar{\alpha})}, \tag{1b}$$

where $\bar{\alpha}$, $\bar{\delta}$ are the centre points of the frame in the α, δ dimensions.

We then fit the first epoch ξ/η positions of all sources in the frame to their corresponding array positions using a third-order polynomial and then applied its inverse to the first and second epoch array positions (both now in the first epoch array coordinate system) to transform them on to first epoch tangent plane. This was simpler than applying the α, δ information in the fits headers to the second epoch data and has a precision better than 1 mas. Creation of a polynomial on which differentiation can be performed from the transformation matrix created in this process is not trivial. It is therefore very difficult to formally propagate the uncertainties through the transformation. Instead, we transformed the array position 1σ error box, the uncertainty being half the difference between these boundaries after the transformation was applied. Calculation of each source's proper motion was then a matter of subtracting the first epoch tangent plane positions from the second epoch tangent plane positions and dividing through by the epoch baseline. The uncertainty on the proper motion is the first and second epoch positional uncertainties added in quadrature and divided by the epoch baseline.

3.6 Relative to absolute proper motion correction

Until this stage, proper motions were relative to the mean motion of the reference sources used for the fit. These were stellar sources which all have a component of proper motion due to Galactic rotation and solar motion. We remove this component of proper motion and convert the relative proper motions to absolute ones, defined by selected extragalactic sources. We calculated the median relative proper motion of sources meeting the following criteria.

Classified as a galaxy in J1 and J2;
J1 and J2 between 12 and 19.6;
J1 and J2 magnitude error <0.2; and
total relative proper motion error $<30\,\mathrm{mas\,yr^{-1}}$.

We used sources in the target frame and those from surrounding frames within 3°. Their median motions were then subtracted from the relative proper motions of all sources in the target frame. We find that using extragalactic sources only in the same frame or using the mean relative motion for all sources within 3° introduces significant local scatter in the correction vectors due to inaccuracies in the centroids of extended objects. Fig. 3 shows how the number of galaxies used varies with sky position. No correction is greater than $10\,\mathrm{mas\,yr^{-1}}$ in $\mu_\alpha\cos\delta$ or $12\,\mathrm{mas\,yr^{-1}}$ in μ_δ. This is typically less than the uncertainties on the motions. Ideally, quasars located in the same frame would be used to calculate the correction; however, we would require a sample of confirmed quasars with several well distributed in each frame. The standard error on the median of the relative proper motion uncertainty of the selected galaxies was then added in quadrature to the uncertainties of the relative proper motions of all sources in the target frame to calculate the uncertainties on the absolute proper motions. The median contribution of the relative to absolute proper motion correction to the absolute proper motion uncertainty is $0.016\,\mathrm{mas\,yr^{-1}}$ in both dimensions.

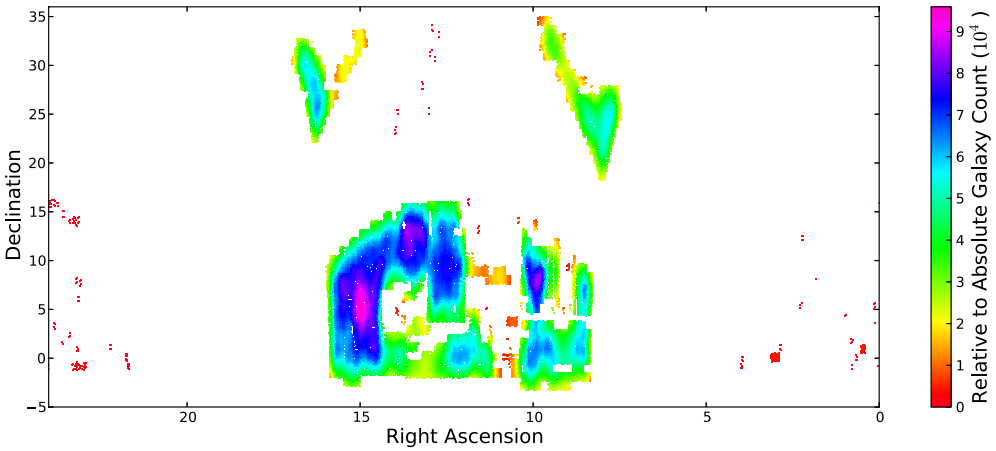

Figure 3. The distribution of the number of galaxies used to calculate the relative to absolute correction of each frame. Relatively few are used in isolated frames; the lowest value is 5. In frames central to the larger fields values can be as high as 95 000.

3.7 Duplicate source removal

The catalogue contained duplicates of sources in regions of overlapping frames. We matched internally for groups of sources with separations less than 1 arcsec using the Tool for Operations on Catalogues And Tables (TOPCAT; Taylor 2005), finding 1614 695 initial groups containing a total of 3380 822 sources. We found that 99.94 per cent of groups with separations of 0.5 arcsec or less contained sources from different frames. We made the assumption that since the overlap of the frames is typically ∼24 arcsec it is unlikely that genuine neighbouring sources would be present only on different frames. Instead, both components of a genuine group would be duplicated. Using this assumption, we remove all but the source with the lowest uncertainty on the total proper motion from groups containing sources from different frames (see Fig. 4). This removed all but the most well-measured source from each set of duplicates, a reduction in catalogue size by 10.6 per cent.

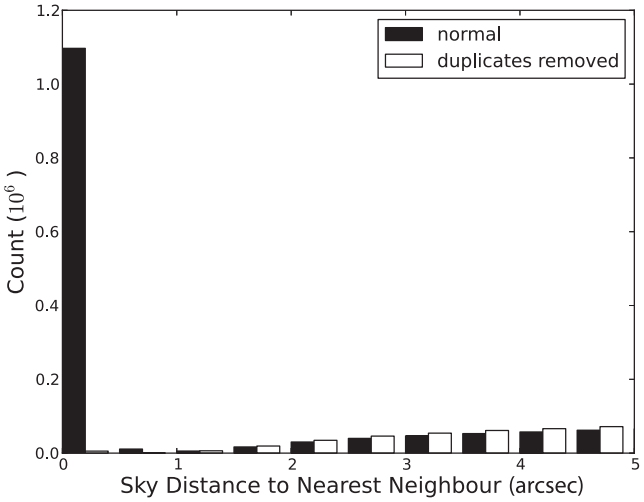

Figure 4. The distribution of distances between sources (within 10 arcsec) before and after application of our duplicate removal method. The huge peak at very low separations and the fact that overwhelming majority of these pairs are in different frames is indicative of duplicate sources in frame overlap regions. After removing these duplicates using the method in Section 3.7 the peak has been almost entirely removed. The remaining sources are close pairs in the same frame set therefore likely to be genuine.

3.8 *YHK* retrieval and bad data removal

We matched LAS 10th data release (DR10) first epoch *J* band equatorial positions and magnitudes retrieved from the WSA las-Detection tables to our catalogue, giving us WSA assigned source IDs and hence a method to accurately match to their source table and retrieve the data contained within. We retrieved *Y*, *H* and *K* magnitudes and their associated uncertainties as well as first and second (where available) epoch *J* band post-processing error bits (ppErrBits[2]) information. ppErrBits is a useful indicator of the quality of each detection, larger values are indicative of more severe detection quality issues. We removed from the catalogue all sources with ppErrBits values of 256 or greater which would correspond to saturation or electronic cross-talk (Dye et al. 2006) or poor flat-field region, etc.

3.9 Bad pixel sources

Approximately 20 per cent of catalogue sources have a '−7' (bad pixel within 2 arcsec aperture) classification at either epoch. We find this has a negative effect on the precision of the astrometry, as one might expect. The median total proper motion for this selection is 50 per cent larger than that of the rest of the catalogue, whereas the mean uncertainty is only 25 per cent larger. We expect the source with the median total proper motion will in reality have a negligible motion and as such the mean uncertainty on the value should be of a similar magnitude. Although the proper motion uncertainties on sources with a bad pixel classification at either epoch were already slightly higher than normal sources (by this factor of about 1.25), we inflated their proper motion uncertainties by a factor of 1.2 to mirror the relative increase in median proper motion by this amount. The distribution of the final uncertainties on absolute proper motions is shown in Fig. 5.

The presence of a '−7' in the classification column means that a genuine classification (−1/1, stellar/extragalactic, etc.) is unavailable. To compensate for this, we include the WSA merged class attribute[3] where available. Merged Class is a combination of classifications in all available bands and epochs of UKIDSS DR10 using Bayesian classification rules.

[2] See http://surveys.roe.ac.uk/wsa/ppErrBits.html
[3] See http://surveys.roe.ac.uk/wsa/www/gloss_m.html#lassource_mergedclass

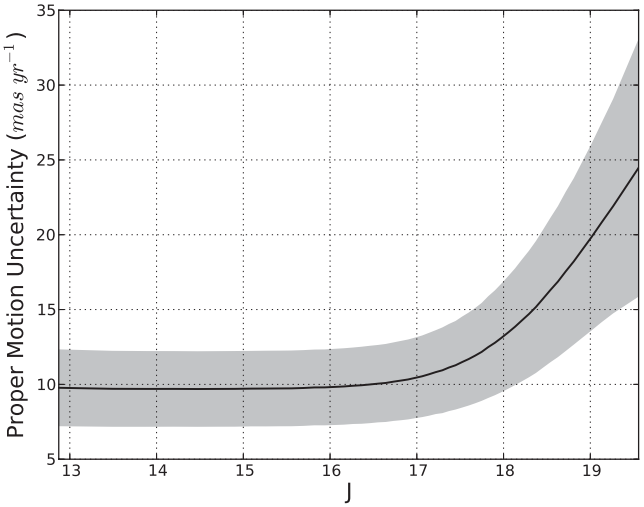

Figure 5. We selected sources meeting the same criteria as in Section 4.1 (5.4 million sources) and split them into 53 J magnitude bins each containing approximately 100 000 sources but having a variable width. The mean uncertainty on $\mu_{\rm total}$ in each bin is plotted. The shaded section shows the region bound by 1 standard deviation.

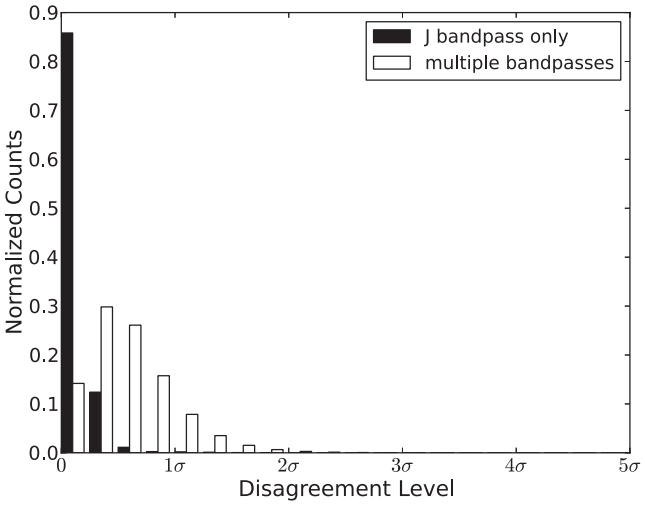

Figure 6. Histogram showing the distribution of disagreement between proper motions of stellar sources from our pipeline and those from the WSA. The catalogues agree very well where the WSA has used only *J* bandpass data for their proper motion, and less well where they have used multiple bandpasses. Pearson product–moment correlation coefficients are 0.99 and 0.80 for J only and multiple bandpass total proper motions, respectively.

We note that since the proper motions of these objects are less reliable they are not used as reference sources at any stage of the pipeline.

4 ANALYSIS OF RESULTS

While we produce results for all LAS sources here we publish only those with absolute proper motions detected at the 5σ level and above, with a morphological classification indicating a likely stellar nature. We include sources classified as stellar (class $= -1$) or probably stellar (class $= -2$) at one or more epochs and exclude sources classed as noise (class $= 0$) at either epoch. We find 135 625 sources classified as stellar in both *J* band detections, and a further 88 324 sources with ambiguous morphological classifications. This produces a catalogue of 223 949 sources in the 1500 deg^2 area shown in Fig. 3. Note that ellipticity and morphological classification trace genuine high proper motion detections very well at $J \leq 19$ (see Section 4.5). However, in the interests of not rejecting large numbers of potentially genuine sources we impose no restriction on ellipticity. We recommend that users employ cuts on ellipticity and morphological classification if a very reliable high proper motion sample is sought. The lowest uncertainties for the brightest and faintest sources are 4 and 12 mas yr^{-1}, respectively, corresponding to the longest epoch baselines. The 5σ lower limit on absolute proper motion significance therefore corresponds to minimum proper motions of 20 to 60 mas yr^{-1} for bright and faint sources, respectively. A sample of the catalogue is presented in the Appendix and the full table is available in the online data.

We scrutinized 1/5th of the results, approximately 300 deg^2. This area corresponds to the overlap with second epoch J coverage of UKIDSS DR10.

4.1 Comparison to WSA proper motions

With the WSA's 9th release of LAS data came proper motions (Collins & Hambly 2012) to which we have compared our results (Fig. 6). The WSA proper motions are not absolute, so here we compare using the relative proper motions calculated by our pipeline. The WSA uses a linear transform in the tangent plane across the whole frame which we have shown in Section 3.4 to be less accurate. It effectively assumes that there are no non-linear distortions in the focal plane apart from the known third-order radial distortion that is removed by the UKIDSS pipeline as part of the astrometric solution for each WFCAM array.

We created and calculated proper motions for a new input data set containing the most recent WSA DR10 data from the LAS detection table. Matching the two catalogues using the unique source IDs assigned by the WSA and maintained throughout our proper motion pipeline ensures there are no mismatches.

We select sources with no post-processing error flags, low ellipticity and classified as stellar in both *J* band images as an appropriate group of sources for comparison, a total of 1.6 million sources.

The proper motion measurements are fairly consistent between the catalogues with Pearson product–moment correlation coefficients of 0.80 and 0.82 in $\mu_\alpha \cos\delta$ and μ_δ, respectively, and 86 and 99 per cent of proper motions matching within their 1σ and 2σ uncertainties, respectively. The WSA proper motions are obtained using all available LAS detections in the *YJHK* passbands. The WSA assumes that chromatic dispersion is minimal, and hence no effort is made to correct for the effects of this. We note that where the WSA results used multiband frames to calculate a proper motion our values differ slightly more, with Pearson's *r* coefficients of 0.79 and 0.82 in $\mu_\alpha \cos\delta$ and μ_δ, respectively. As one might expect, for the few sources with only *J* band images the proper motions agree very well, with Pearson's *r* coefficients of 0.99 in both $\mu_\alpha \cos\delta$ and μ_δ.

4.2 Comparison to LSPM catalogue

The LSPM catalogue (Lépine & Shara 2005) utilizes the SUPERBLINK software (Lépine, Shara & Rich 2002) to normalize the differences between pairs of subframes from the POSS-I (Abell 1959) and POSS-II (Reid et al. 1991) plates (usually involving a degradation in the quality of the POSS-II plate to match the POSS-I plate quality), then the subtraction of one from the other to produce a residual

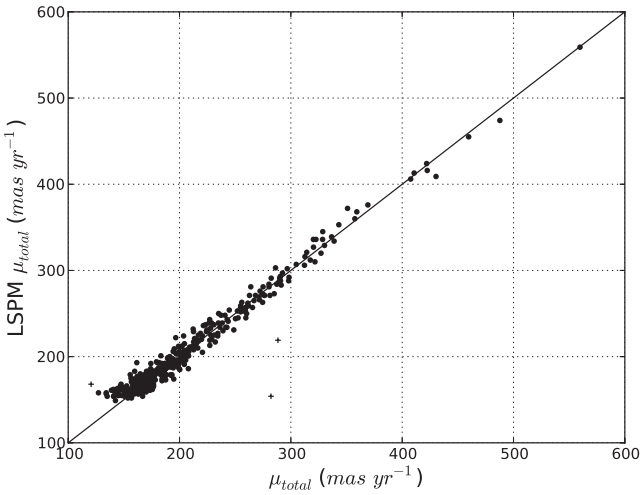

Figure 7. LSPM total proper motions (vertical axis) versus those calculated by our pipeline (horizontal axis) for the 381 matches between the two catalogues. The crosses are LSPM J1644+3203, LSPM J1625+2519 and LSPM J1609+2457 for which the total proper motions differ greater than 4σ. The data are nevertheless well correlated; the Pearson product–moment correlation coefficient is 0.980.

image, which maps the first and second epoch positions of sources with high proper motion. The catalogue benefits from the fact that all high proper motion sources identified by the SUPERBLINK software were manually blinked to remove any erroneous high proper motion sources, the LSPM catalogue has a minimal false detection contamination as a result. The LSPM catalogue also includes data from the Tycho-2 (Høg et al. 2000) catalogue and the All-Sky Compiled Catalogue (Kharchenko 2001).

We matched the LSPM-North catalogue to our LAS proper motion catalogue using a 3 arcsec matching radius and a 0.5 mag *J* band discrepancy tolerance. We find 381 matches and compare LSPM and our LAS proper motions, see Fig. 7. The majority of LSPM proper motions given are derived using the author's SUPERBLINK software, there is one Tycho-2 proper motion and four from 'other' sources, these five proper motions agree well with those from our LAS catalogue. We found proper motions from both catalogues agreed within their 1σ uncertainties for 79 per cent of sources, this rises to 98 per cent agreement at 2σ. The LSPM proper motion uncertainties were taken as 8mas yr^{-1} (Lépine & Shara 2005). The proper motions are also well correlated, with Pearson product–moment correlation coefficients of 0.994, 0.979 and 0.980 ($\mu_\alpha \cos\delta$, μ_δ and $\mu_{\rm total}$, respectively). Statistically, from a sample of 381 sources we do not expect any to have proper motions with a disagreement greater than 4σ, we find 3: LSPM J1644+3203, 4.43σ; LSPM J1625+2519, 4.81σ; and LSPM J1609+2457, 27.41σ.

LSPM J1644+3203

In the J1 image the high proper motion source is overlapping another source to the north with a separation of 1.3 arcsec. This is probably causing the centroid on the object at J1 to be skewed north causing the observed larger proper motion in declination. The proper motion in right ascension agrees comfortably. LSPM J1644+3203 is NLTT 43473 (see Section 4.3) which has a proper motion in agreement with the LSPM catalogue.

LSPM J1625+2519

On inspection of the two epochs of UKIDSS LAS *J* band images the source is separated by 1.7 arcsec from another source, which was unresolved in the photographic data. Plotting the positions of the centroids at both epochs shows that at the second epoch the centroids are well fitted to both sources. The first epoch image quality is slightly lower which caused the fainter target to go undetected and the centroid for LSPM J1625+2519 to be skewed towards it, altering the measured proper motion. Interestingly, the source which is overlapping LSPM J1625+2519 appears to share a common proper motion with it.

LSPM J1609+2457

While blinking the two epochs of UKIDSS LAS images the source does appear at first glance to exhibit a proper motion consistent with our value, we note that the quality of the first epoch *J* band image is poor. Blinking of the POSS-I and POSS-II images reveals a motion consistent with the value given in the LSPM catalogue. No other source with a proper motion consistent with LSPM J1609+2457 is found in our catalogue within 1 arcmin of its given location. The cause of this erroneous proper motion measurement is likely the poor first epoch UKIDSS *J* band image and resultant centroid fit. Since the LAS proper motion is likely to be the incorrect proper motion measurement we have included this source in our comparison.

We attribute the presence of the poor quality images mentioned above to our use of data that have not yet been through the UKIDSS quality control procedures that take place prior to a formal SQL data release. We note that this has probably been the cause of two of the erroneous proper motions from this sample of 381.

In an effort to gauge the completeness of the catalogue we identified LSPM sources within the UKIDSS DR10 area and with 2MASS J magnitude > 12.5. The J magnitude cut includes null values and allows for a half a magnitude discrepancy between the UKIDSS and 2MASS *J* band magnitudes, this is necessary to accommodate recovery of UKIDSS objects measured up to half a magnitude brighter than in 2MASS, which would otherwise appear unrecovered due to our 12th magnitude bright limit. We identify 379 LSPM sources that should be present within this catalogue, of which we recover 375 with proper motions that agree within 4σ. A further three sources have discrepant proper motions, these are LSPM J1644+3203, LSPM J1625+2519 and LSPM J1609+2457 (see above). The final unrecovered source is LSPM J0829+2539/LHS 2015. LHS 2015 is a previously unresolved common proper motion pair originally classified by Reid & Gizis (2005) as a DQ white dwarf. The pair is unresolved in the first epoch *J* band image and is consequentially more than half a magnitude brighter than the resolved magnitudes at the second epoch. This caused the pair to fail this quality control cut at the epoch matching stage. If we consider sources with discrepant proper motions as unrecovered then we have an LSPM source recovery rate of 98.9 per cent, otherwise the recovery rate is 99.7 per cent.

Fig. 8 compares the number of high proper motion (>150 mas yr^{-1}) sources fainter than $J = 12$ as a function of J magnitude in the UKIDSS DR10 area from our catalogue and the LSPM. We require sources in our catalogue to have ellipticity < 0.3 and be classified as stellar at both epochs. This requirement means we can infer an approximate false positive rate from Fig. 12, at the likely expense of some genuine detections. The LSPM catalogue is more complete at the bright end, where our catalogue suffers from

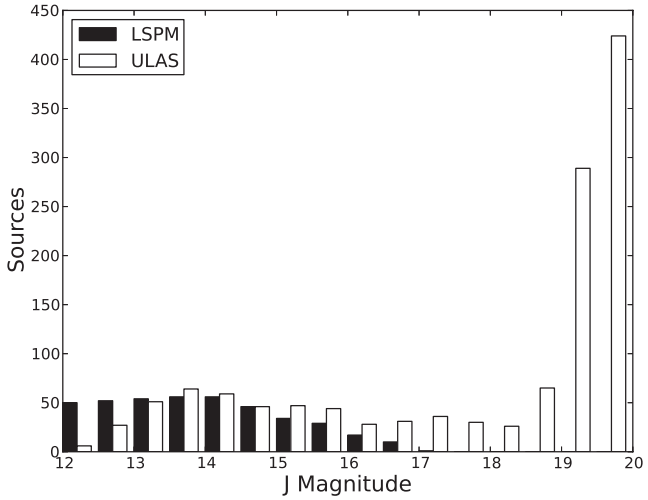

Figure 8. A comparison between the number of LSPM high proper motion stars and those from this catalogue after application of ellipticity and morphological classification cuts (see the text). Note that the false positive rate of the ULAS high proper motion detections increases sharply at $J \sim 19$. Our catalogue is more complete fainter than $J = 13.5$.

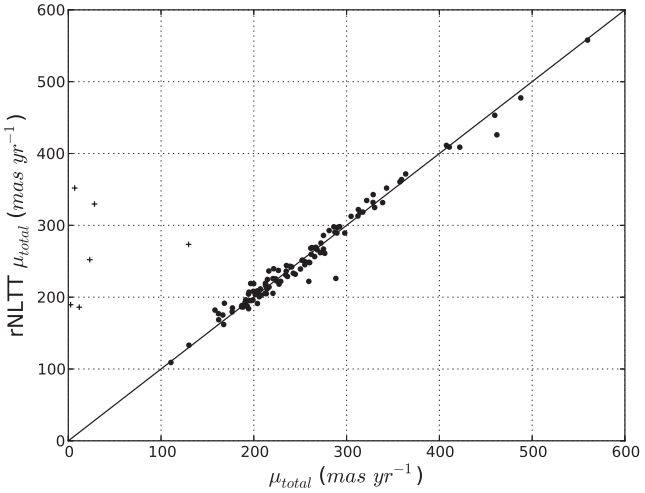

Figure 9. Comparison between proper motions from the rNLTT catalogue (vertical axis) and those calculated by our pipeline (horizontal axis) for the 109 reliable matches between the catalogues. The six sources represented by crosses are those with proper motions differences greater than 2σ listed in Section 4.3, these were removed from the comparison since they were found to have spurious rNLTT proper motion values. The Pearson product–moment correlation coefficient for the remaining data is 0.988.

near saturation. We begin to find more high proper motion sources than the LSPM catalogue at about $J = 13.5$. The false positive rate of ULAS sources increases sharply at around $J = 19$ (see Fig. 12) which must be taken into account, and that 25 LSPM sources (6 per cent) have null J band magnitudes and therefore could not be included in the comparison. The decline in source counts in our catalogue at $J \geq 13.5$ we believe is due to the increasing average distance, and hence smaller average proper motion of these relatively faint stars.

4.3 Comparison to revised NLTT catalogue

The Luyten Half Second (LHS) catalogue contains stars with proper motions exceeding 0.5 arcsec annually (Luyten 1979a). The LHS catalogue contains positions, proper motions and optical magnitudes for 4470 stars with proper motions greater than 239 mas yr^{-1} (note that a small number of sources were included, in spite of the 0.5 arcsec yr^{-1} lower limit). The catalogue includes data compiled from other proper motion searches and 804 hand/machine-blinked Palomar Sky Survey fields. The LHS catalogue was revised by Bakos, Sahu & Németh (2002). 4323 of the original 4470 high proper motion sources were recovered and their positions and proper motions were refined.

The New Luyten catalogue of stars with proper motions larger than Two Tenths of an arcsecond (NLTT; Luyten 1979b) catalogue is an extension of the LHS catalogue down to proper motions of 40 mas yr^{-1} for 58 845 sources. A minority (152) have proper motion less than 180 mas yr^{-1}, however. The NLTT catalogue was revised and refined by Salim & Gould (2003), giving improved positions and proper motions for sources present in both the original POSS-I frames and the second 2MASS data release.

We matched the revised NLTT (rNLTT) catalogue (Salim & Gould 2003) to our LAS proper motion catalogue using the same matching criteria as for the LSPM comparison (section 4.2), this time finding 115 initial matches, see Fig. 9. We find proper motions from both catalogues agreed within their 1σ uncertainties for 70 per cent of sources, rising to 94 per cent agreement at 2σ. The remaining seven sources have proper motion disagreements of greater than their 4σ uncertainties: NLTT 43473, 4.73σ; NLTT 22010, 6.22σ; NLTT 21214, 9.36σ; NLTT 20123, 10.14σ; NLTT 18649, 21.01σ; NLTT 18692, 21.52σ; and NLTT 19021 26.74σ. We visually inspected the POSS-I and POSS-II photographic plate scans to investigate the cause of these differences in proper motion. We find all but NLTT 43473 and NLTT 20123 to have incorrect J2000 position measurements and all but NLTT 43473 have spurious proper motion values upon comparison to other proper motion catalogues. Pearson product–moment correlation coefficients are 0.998, 0.995 and 0.988 $\mu_\alpha \cos\delta$, μ_δ and $\mu_{\rm total}$, respectively, after removal of the six sources as discussed below.

NLTT 43473

In the J1 image, the high proper motion source is overlapping another source to the north with a separation of 1.3 arcsec, likely causing the centroid on the object at J1 to be skewed north and further causing the observed larger proper motion in declination. Proper motion in right ascension agrees comfortably. Since this is a genuine match and the rNLTT proper motion is corroborated by the LSPM catalogue we have included it in the comparison.

NLTT 22010

No high proper motion object is observed during blinking of 3 arcmin × 3 arcmin UKIDSS images, in agreement with our proper motion results. We included the 2MASS image in blinking and still no high proper motion object is evident. No source in our catalogue has a similar proper motion within 1 arcmin of the given position of NLTT 22010. We can see no source with stated rNLTT 22010 proper motion when blinking 12 arcmin × 12 arcmin POSS-I and POSS-II images (with a 42 year baseline the total expected movement is 7.8 arcsec which should be clearly visible). Also note that this source is not present in LSPM match even though its area should be covered. This high proper motion source is therefore questionable and it has been removed from our comparison.

NLTT 21214

Inspection of 1 arcmin × 1 arcmin UKIDSS images centred on the rNLTT J2000 position of NLTT 21214 reveals the UKIDSS source as clearly extended and no proper motion, in agreement with our catalogue and consistent with the source being extragalactic. We located NLTT 21214 approximately 1.25 arcmin to the north-east of the Salim & Gould (2003) given J2000 position. Furthermore, the magnitude of the rNLTT proper motion for this source (−75 and −174 mas yr^{-1} in $\mu_\alpha \cos\delta$ and μ_δ, respectively) is not in agreement with the LSPM catalogue (−114 ± 8 and −217 ± 8 mas yr^{-1} in $\mu_\alpha \cos\delta$ and μ_δ) or our own (−123 ± 9 and −228 ± 8 mas yr^{-1} in $\mu_\alpha \cos\delta$ and μ_δ). The original NLTT proper motion is closer (−104 and −195 mas yr^{-1} in $\mu_\alpha \cos\delta$ and μ_δ). This source has been removed from the comparison due to a suspected incorrect rNLTT proper motion.

NLTT 20123

High proper motion evident on blinking of UKIDSS and POSS images, direction of proper motion is in agreement with rNLTT and our catalogue. A rough centroid on the source at both epochs using the region tool in DS9 and the world coordinate system information contained in the image headers gives proper motions of 54 and −102 mas yr^{-1} in RA and Dec., respectively, consistent with our catalogue values. USNO-B1.0 and LSPM proper motion values are also consistent with our catalogue. No source in our catalogue has a similar proper motion within 2 arcmin of the given position of NLTT 20123. We suspect the rNLTT proper motion of this source is incorrect and have removed it from our comparison.

NLTT 18649

We blinked POSS-I (R band) and POSS-II (IR) images with an epoch baseline of 48 years and located NLTT 18649 1.4 arcmin south–south-west of Salim & Gould (2003) J2000 location. We located NLTT 18649 in our catalogue with a proper motion not in agreement with rNLTT but agreeing well with LSPM and USNO-B1.0 values. We suspect the rNLTT proper motion of this source is incorrect and have removed it from our comparison.

NLTT 18692

We located NLTT 18692 1.25 arcmin south-west–west of Salim & Gould (2003) J2000 location. The rNLTT proper motion for 18692 is inconsistent with the USNO-B1.0 and LSPM catalogue values and has been removed from this comparison as a result. The LSPM and USNO-B1.0 proper motion values agree well with those of our catalogue.

NLTT 19021

We located NLTT 19021 1.4 arcmin south–south-east of Salim & Gould (2003) J2000 location. The rNLTT proper motion for 19021 is inconsistent with the USNO-B1.0 and LSPM catalogue values and has been removed from this comparison as a result. Note that the LSPM and USNO-B1.0 proper motion values agree very well with those of our catalogue.

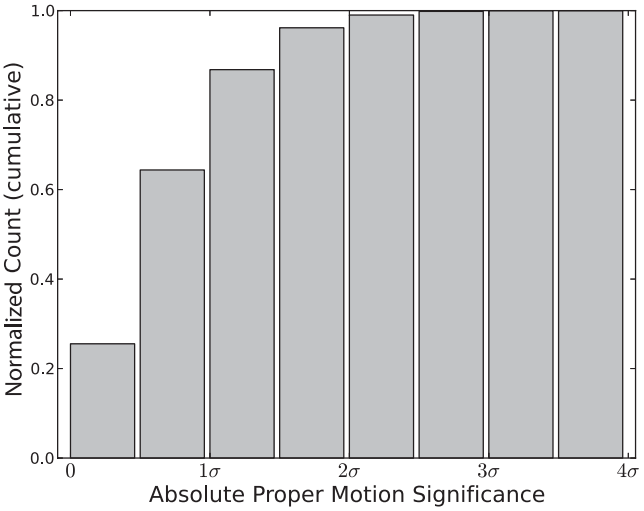

Figure 10. We identified 4661 quasars within our catalogue using a method described in Section 4.4. This plot shows the distribution of the proper motion significance of the quasar sample.

4.4 Testing the relative to absolute correction

We produced a list of quasar candidates by matching the full catalogue to the Large Quasar Reference Frame (LQRF; Andrei et al. 2009) using a 1 arcsec matching radius. We rejected quasar matches with more than one ULAS source within 3 arcsec and any that did not meet the restrictions imposed on reference stars described in Section 3.3, leaving 4661 quasar candidates. The mean absolute proper motion of this sample is −0.44 ± 0.16 and −0.08 ± 0.15 mas yr^{-1} in $\alpha\cos\delta$ and δ, respectively. While the mean absolute proper motion of this sample in $\alpha\cos\delta$ is significant at the 2.75σ level, we note that it is much smaller than the typical uncertainties on the proper motions (see Fig. 5). Fig. 10 shows the distribution of proper motion significances for this sample.

We selected a sample of 214 593 sources with which to test the direction and magnitude of the relative to absolute correction. Sources were selected in absolute proper motion space such that their motions were greater than three times their error and less than 500 mas yr^{-1}, since we wanted to exclude the nearest sources, for which random velocity dispersion is the dominant factor in their proper motion, as opposed to Galactic location. We also selected only sources with 16 < J1 and J2 < 19.6, J1 and J2 uncertainty < 0.1, J1 and J2 ellipticity < 0.3, and classified as stellar at both epochs. We binned the sample in 13° × 13° bins ($l \times b$), rejecting any bins containing fewer than five sources. Proper motions were converted into the Galactic coordinate system and the median motion of each bin was calculated. Fig. 11 shows the median motions in Galactic coordinates, which agrees well with an equivalent plot derived from *Hipparcos* measurements in Abad et al. (2003, their fig. 4). The points with Galactic latitude $b < 0°$ are those of the isolated fields which have very low relative to absolute correction reference galaxy counts (see Fig. 3). While the UKIDSS LAS and this catalogue were not designed to improve on the values of Oort's constants, using our sample we derive a value of −13.79 ± 6.58 km s^{-1} kpc^{-1} for the B constant. This agrees with a value of −12.37 ± 0.64 km s^{-1} kpc^{-1} derived from *Hipparcos* measurements by Feast & Whitelock (1997) and should therefore validate our relative to absolute correction. The A constant in our case is related to radial velocity and hence a well-constrained A constant is difficult to obtain.

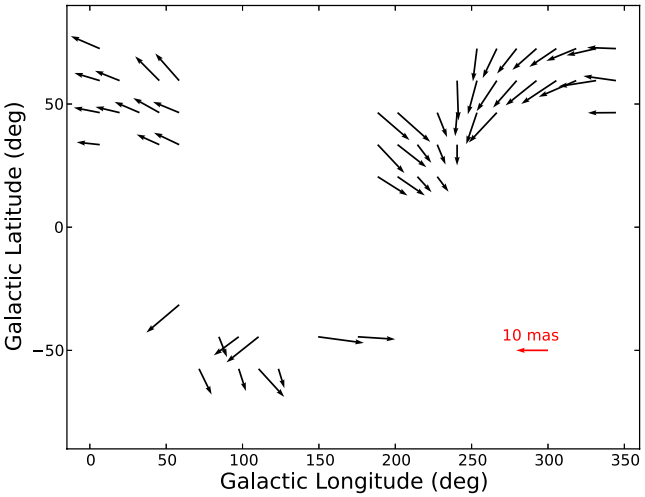

Figure 11. Median proper motions in Galactic coordinates of a sample of 214 593 sources with well-measured proper motions. The sample was separated into 13° × 13° ($l \times b$) bins. The red arrow shows an example motion of magnitude 10 mas. The points with Galactic latitude $b < 0°$ are those of isolated fields which suffer from a relative lack of reference galaxies.

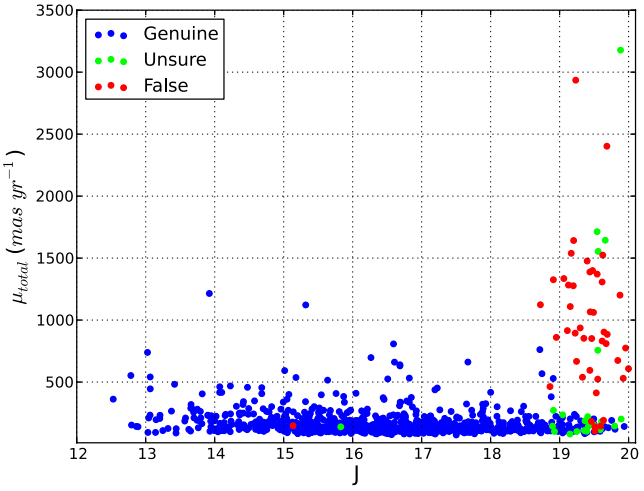

Figure 12. The distribution of *genuine*, *false* and *ambiguous* high proper motion candidates from Section 4.5 in proper motion and *J* band brightness.

4.5 Investigation of faint limit

To attempt to quantify the reliability of catalogue proper motions and provide a reliable sample of brown dwarf candidates for binary searches (see Section 5.5.3) we blinked all 980 sources with motions of 500 mas or more that also met the following criteria:

$Y - J > 0.7$;
J1 and J2 ellipticity < 0.3;
J1 and J2 classification -1 (stellar);
mergedClass $= -1$ (stellar).

We assigned classifications of genuine, false and unsure based on their calculated motion compared to their apparent motion. If there appeared to be another object in the 1 arcmin × 1 arcmin field with roughly the same motion vector then the target was flagged as interesting (see Section 5.5.3). We chose a minimum motion between epochs of 500 mas since a motion of this magnitude should be detectable by eye, covering 2.5 pixels between the LAS *J* band images.

First epoch images were obtained using the multiGetImage tool of the WSA and we wrote Linux scripts to retrieve second epoch *J* band images via the WSA Archive Listing tool. A further shell script was used to automatically select pairs of images and blink them using DS9, which made visual inspection of this sample of almost one thousand images possible in a day.

Fig. 12 shows the distribution of genuine, false and ambiguous proper motions for this sample in proper motion and brightness. We find the catalogue to be very reliable for red sources brighter than $J = 19$. Reliability is diminished at the faint end but there are still many genuine high proper motion sources that can be found. We find a total of 834 genuine high proper motion sources in this sample. We note that the vast majority of false high proper motions were due to mismatched sources, which is to be expected due to the 0.5 J magnitude variability tolerance and given the increase in source density towards the faint end.

4.6 Catalogue caveats

We find that ULAS sources brighter than 12 in J are often either saturated or very close to saturation and their centroids often fall in different places at different epochs and wavebands. This causes false high proper motions and large differences between the WSA proper motion values and ours. The vast majority of saturated objects were identified and flagged by the WSA and then removed from our catalogue by us, though further investigation showed that a few remained and as a result we elected to remove all sources brighter than 12 in the *J* band. We also find diffraction spikes of very bright stars as false high proper motion objects. Where these are not identified by the CASU/WSA pipelines they are usually identifiable as having large ellipticities and are easy to screen for through visual inspection, the pdf document report generated by the multiGetImage tool of the WSA in standard mode is sufficient in most cases.

Ideally, quasars should be used for a relative to absolute correction but we would require several well distributed about each frame. A simple 1 arcsec match to the LQRF (Andrei et al. 2009) yields one quasar for every two LAS frames on average which is insufficient for our purposes. Therefore, we used galaxies as described in Section 3.6.

Relative proper motions are relative to the average motion of the reference stars used to compute the polynomial transform. Where a local transform is used, the zero-point motion is never exactly the same. This may introduce a small systematic random error into the absolute proper motion since the correction vectors are applied globally. Steps have been taken to limit this: only sources with small preliminarily measured residuals are used as reference sources in the final fit; and the requirement of at least three reference sources in each quadrant means that a minimum of 12 reference sources are used. This should be sufficient to reduce any scatter in global–local mean motions. Indeed, we find that the mean difference between global and local residuals for bright stars is 13 mas on each axis, which is only 20 per cent of the typical uncertainty on the residuals. Visual inspection of the spatial distribution of local–global variation shows no serious anomalies.

Sources LSPM J1625+2519 and LSPM J1609+2457 were found in our catalogue with proper motion measurements inconsistent with those of the LSPM catalogue (see Section 4.2). An inspection of the *J* band UKIDSS images indicated that the source of these

inconsistent proper motions may be a poor quality UKIDSS frame for each leading to an inaccurate centroids on the sources at those epochs. This is probably due to the inclusion of a small number of poor quality UKIDSS images because much of the second epoch data have not yet been through the UKIDSS quality control procedures. We note however that 99.5 per cent of sources compared were unaffected by this and it is as such a minor issue.

5 RESULTS

To capitalize on the availability of proper motions and a wide range of photometry for a large fraction of the LAS field we undertook several searches for new high proper motion objects which we detail here. Results of searches for new benchmark UCDs can be found in Section 6. Note that unless stated otherwise *Y*, *J*, *H* and *K* magnitudes in this section are on the Mauna Kea Observatory (MKO) system and *J* band photometry is UKIDSS first epoch. We give first epoch J magnitude since it is most often contemporaneous with the *Y*-band observation.

5.1 Initial searches for interesting high proper motion objects

In a further effort to gauge the reliability of the catalogue to search for new high proper motion objects, we selected a group of bright high proper motion objects from the 300 deg^2 of overlap with UKIDSS DR10 that also met the following restrictions:

J1 $<$ 18;
J1 and J2 ellipticity $<$0.3;
J1 and J2 classification -1 (stellar);
total proper motion $>$300 mas yr^{-1}.

Note that there were no colour constraints in this selection. The selection left us with 42 sources to investigate. We retrieved their first and second epoch *J* band FITS images from the WSA using the multiGetImage tool and cross-matched with SIMBAD to get names and alternative proper motions where available. We also cross-matched to the SDSS DR9, which we verified visually, to retrieve *ugriz* optical photometry. Their images were blinked to verify their high proper motions. The values determined are given in Tables 1 and 2. We note that one source is false (discussed below) and is therefore not included in these tables.

Here we itemize sources of interest amongst the 41 bright, high proper motion sources.

LSR J0745+2627

This object was selected as one of the highest proper motion sources in a prototype version of this catalogue based on UKIDSS LAS DR9 data. It has previous proper motion measurements by Lépine & Shara (2005) and white dwarf identification by Reid (2003). Using this catalogue, LSR J0745+2627 was re-identified by Catalán et al. (2012) as the brightest pure-H ultracool ($T_{\rm eff} < 4000$ K) white dwarf currently known.

LHS 6139 and ULAS J081127.84+203925.7

These objects share a common proper motion (see Fig. 13). The difference in their measured proper motions is half its uncertainty.

ULAS J082155.56+250939.8

The T4.5 dwarf ULAS J082155.56+250939.8, confirmed with a Gemini Near InfraRed Imager and Spectrometer spectrum, identified by Burningham et al. (2013).

2MASS J07414920+2351275

The T5 dwarf (Burgasser et al. 2006) 2MASS J07414920+2351275 has a proper motion discrepancy between our catalogue and previous measurements by Casewell et al. (2008) (-250.22 ± 12.18 and -116.21 ± 13.32 mas yr^{-1} in RA and Dec., respectively) and Faherty et al. (2009) (-243 ± 13 and -143 ± 14 mas yr^{-1} in RA and Dec., respectively). Faherty et al. (2009) also provide a distance of 18 ± 2 pc for this object. There is no obvious defect present in the two *J* band images which might cause such an error in the proper motion. The relatively large parallax of the source can be ruled out as the source of proper motion error in our catalogue since our epoch baseline is 11 d from a year. We also find that the WSA proper motion, derived from detections in all five bands, is consistent with our value. The source of this discrepancy remains unknown.

2MASS J08044064+2239502 & NLTT 42650

Identified by Kilic et al. (2010), the DZ white dwarf 2MASS J08044064+2239502 and the DC white dwarf NLTT 42650.

EGGR 531

The well-studied DA8 white dwarf EGGR 531, first identified by Greenstein (1980).

LP 260−3, 2MASS J15593876+2550362 and LSPM J1641+3210

The M2, M6 and M7 type dwarfs LP 260−3, LSPM J1641+3210 and 2MASS J15593876+2550362 are previously studied separate systems. Spectral types, photometric distances (508, 55.9 and 161.9 pc) and radial velocities (105, -6.1 and -54.7 km s^{-1}) were measured by West et al. (2008) using their respective SDSS DR5 spectra.

WD 0921+315

The $4810 \pm 60K$ DC helium-rich white dwarf WD 0921+315 identified by Sayres et al. (2012). The SDSS spectrum provides spectroscopic confirmation.

ups Gem ghost

A ghosted image of ups Gem (see Fig. 14) is the only false high proper motion (-224 ± 10 & -1547 ± 9 mas yr^{-1} in $\mu_\alpha \cos\delta$ and μ_δ, respectively) source to have escaped rejection by the cuts described above. Suggesting that while they are effective at removing a lot of false high proper motion sources some will remain. If a clean high proper motion sample is required then blinking the first and second epoch *J* band images is recommended where practical. Images may be retrieved and blinked quickly using the WSA multiGetImage tool and an image viewer which accepts command line input such as DS9.

Table 1. Astrometry for 41 genuine high proper motion (> 300 mas yr^{-1}) sources from our proper motion catalogue. Coordinates are those of the UKIDSS LAS (J1 epoch), converted to 2000.0 epoch using the stated proper motion values. Proper motions are given in units of mas yr^{-1}.

Name	α_{J2000}	δ_{J2000}	$\mu_\alpha \cos\delta$	μ_δ	alt. $\mu_\alpha \cos\delta$	alt. μ_δ	alt. μ source
LP 365−11	07:28:25.75	+24:31:51.9	136 ± 6	−315 ± 6	148 ± 8	−321 ± 8	LSPM
LP 65−25	07:35:02.85	+24:57:04.4	201 ± 5	−251 ± 6	199 ± 8	−238 ± 8	LSPM
2MASS J07414920+2351275	07:41:49.18	+23:51:27.8	−262 ± 11	−212 ± 9	−250 ± 12	−116 ± 13	[a]
LSR J0745+2627	07:45:08.95	+26:27:06.4	527 ± 12	−719 ± 13	496 ± 8	−744 ± 8	LSPM
2MASS J07474639+2605167	07:47:46.39	+26:05:17.5	−189 ± 9	−245 ± 10	−253 ± 49	−170 ± 50	[b]
LP 366−18	07:49:17.18	+21:03:35.8	69 ± 9	−304 ± 9	65 ± 8	−299 ± 8	LSPM
LHS 1953	07:52:08.12	+27:00:01.5	609 ± 7	−658 ± 8	604 ± 8	−667 ± 8	LSPM
LP 366−27	07:56:40.85	+23:36:35.6	74 ± 7	−305 ± 7	93 ± 8	−307 ± 8	LSPM
2MASS J08044064+2239502	08:04:40.63	+22:39:49.7	12 ± 10	−320 ± 11	4 ± 8	−336 ± 8	LSPM
LP 424−14	08:09:40.24	+19:32:04.3	−396 ± 7	−109 ± 6	−398 ± 8	−110 ± 8	LSPM
ULAS J081045.24+222841.9	08:10:45.25	+22:28:44.1	−20 ± 10	−306 ± 8	–	–	–
ULAS J081127.84+203925.7	08:11:27.82	+20:39:28.4	40 ± 8	−460 ± 8	–	–	–
LHS 6139	08:11:27.90	+20:39:26.2	32 ± 8	−461 ± 8	37 ± 8	−467 ± 8	LSPM
G 40−12	08:13:24.20	+26:57:10.6	351 ± 11	−253 ± 7	340 ± 8	−259 ± 8	LSPM
LP 367−56	08:16:36.29	+23:06:16.1	96 ± 8	−344 ± 5	84 ± 8	−350 ± 8	LSPM
EGGR 531	08:16:42.05	+21:37:36.0	−93 ± 9	−397 ± 6	−104 ± 8	−392 ± 8	LSPM
ULAS J082155.56+250939.8	08:21:55.79	+25:09:40.2	−448 ± 11	−62 ± 14	–	–	–
LHS 2006	08:23:47.97	+24:56:57.7	237 ± 6	−479 ± 7	235 ± 8	−471 ± 8	LSPM
2MASS J08253258+2359306	08:25:32.59	+23:59:30.6	−6 ± 7	−327 ± 7	15 ± 8	−320 ± 8	LSPM
LP 311−21	08:28:35.05	+26:45:33.1	193 ± 11	−251 ± 11	199 ± 8	−239 ± 8	LSPM
2MASS J08332144+2300120	08:33:21.45	+23:00:11.8	65 ± 7	−314 ± 10	72 ± 8	−319 ± 8	LSPM
LSPM J0836+2432	08:36:18.07	+24:32:56.7	238 ± 10	−499 ± 13	231 ± 8	−496 ± 8	LSPM
LP 321−30	08:46:01.27	+27:23:07.5	−108 ± 11	−447 ± 5	−103 ± 8	−443 ± 8	LSPM
ULAS J085335.33+285902.4	08:53:35.59	+28:59:07.0	−471 ± 20	−629 ± 11	–	–	–
LP 260−3	09:16:06.52	+32:56:03.0	−229 ± 8	−238 ± 7	−236 ± 8	−229 ± 8	LSPM
LP 313−36	09:17:43.21	+30:56:50.9	−23 ± 8	−304 ± 6	−21 ± 8	−306 ± 8	LSPM
WD 0921+315	09:24:30.86	+31:20:33.6	−204 ± 13	−369 ± 10	−193 ± 8	−378 ± 8	LSPM
2MASS J15052821+3115037	15:05:28.21	+31:15:02.9	−20 ± 6	−512 ± 7	−37	−529	[c]
LP 272−48	15:10:38.43	+33:10:16.9	−43 ± 7	−361 ± 7	−45 ± 8	−365 ± 8	LSPM
LP 327−24	15:11:51.21	+30:33:06.2	−397 ± 8	−283 ± 8	−393 ± 8	−265 ± 8	LSPM
ULAS J151354.98+303543.9	15:13:54.91	+30:35:46.2	156 ± 8	−421 ± 9	–	–	–
LHS 3042	15:14:26.02	+30:23:34.0	−583 ± 9	−9 ± 7	−603 ± 8	−5 ± 8	LSPM
LHS 3063	15:21:51.72	+30:48:26.2	−412 ± 8	341 ± 8	−413 ± 8	339 ± 8	LSPM
2MASS J15593876+2550362	15:59:38.80	+25:50:36.3	−358 ± 10	108 ± 10	−328 ± 37	119 ± 37	[b]
ULAS J160036.59+284305.7	16:00:36.70	+28:43:04.2	−228 ± 13	228 ± 12	–	–	–
NLTT 41963	16:05:52.82	+25:11:38.8	−337 ± 7	−5 ± 7	−339 ± 8	−4 ± 8	LSPM
NLTT 42004	16:06:35.73	+24:28:40.9	−93 ± 5	−309 ± 4	−86 ± 8	−325 ± 8	LSPM
NLTT 42650	16:22:40.15	+29:19:13.0	−298 ± 8	−226 ± 9	−296 ± 8	−218 ± 8	LSPM
LP 330−15	16:26:24.56	+28:56:26.0	−151 ± 9	−304 ± 9	−152 ± 8	−298 ± 8	LSPM
LHS 3198	16:27:40.18	+29:27:15.1	−173 ± 7	−532 ± 8	−156 ± 8	−537 ± 8	LSPM
LSPM J1641+3210	16:41:43.41	+32:10:39.0	−350 ± 6	29 ± 6	−370 ± 8	37 ± 8	LSPM

[a]Casewell, Jameson & Burleigh (2008).
[b]Zhang et al. (2010).
[c]Sheppard & Cushing (2009), stated total proper motion uncertainty is about 10 per cent.

ULAS J075015.48+203650.0

This object was missing from the above selection due to its second *J* band epoch classification as a galaxy, but was identified in other searches. Based on the Hawley et al. (2002) $i - J$ colour to spectral type table and the source's SDSS DR7 *i* band magnitude of 21.21 ± 0.09 (note that the source is missing from SDSS DR8 and DR9), it is a candidate M6/M7 dwarf at a distance of between 260 and 370 pc. It has a 504 ± 18 mas yr^{-1} proper motion. This corresponds to a range of tangential velocities between 620 and 870 km s^{-1}, above the Galactic escape velocity.

5.2 White dwarfs

Ultracool white dwarfs are among the oldest objects in the Galaxy. Their ages are often very well constrained due to their predictable cooling rate based on theoretical models (e.g. Hansen 1999; Meng, Yang & Li 2010), dwarf mass to progenitor star mass relationship and main-sequence progenitor lifetime. Hence, these objects are ideal tools for placing lower limits on the age of the Galaxy and can give us clues to the conditions of a young Milky Way (Kilic et al. 2006). A number of cool white dwarfs have been discovered to date, the usual method of discovery is photometric and reduced proper motion selection (Kilic et al. 2005; Leggett et al. 2011), often followed by spectroscopic confirmation.

For identification of white dwarfs in this catalogue, a cross-match with optical catalogues will be necessary. We identify white dwarf candidates using a combination of cuts on near-infrared and optical (SDSS) colours, proper motion and reduced proper motion, and other selections based on classification and ellipticity designed to reject possible false positives. Our candidates are likely cool white dwarfs based on fits of their photometry to model spectra. We refer

Table 2. SDSS optical and UKIDSS near-infrared photometry for 41 high proper motion ($> 300\,\mathrm{mas\,yr^{-1}}$) sources from our proper motion catalogue. *J* band magnitude is first epoch UKIDSS LAS.

Name	*u*	*g*	*r*	*i*	*z*	*Y*	*J*	*H*	*K*
LP 365−11	20.59 ± 0.05	17.98 ± 0.01	16.59 ± 0.01	16.02 ± 0.01	15.73 ± 0.01	14.980 ± 0.004	14.525 ± 0.010	14.043 ± 0.004	13.865 ± 0.004
LP 65−25	20.17 ± 0.05	17.62 ± 0.01	16.24 ± 0.00	15.67 ± 0.00	15.34 ± 0.01	14.581 ± 0.003	14.178 ± 0.010	13.673 ± 0.003	13.448 ± 0.004
2MASS J07414920+2351275	25.44 ± 0.63	24.31 ± 0.43	24.34 ± 0.52	24.85 ± 0.41	19.56 ± 0.06	17.129 ± 0.013	15.880 ± 0.010	16.104 ± 0.023	16.277 ± 0.037
LSR J0745+2627	22.65 ± 0.24	19.99 ± 0.02	18.69 ± 0.01	18.23 ± 0.01	17.96 ± 0.02	17.389 ± 0.014	17.122 ± 0.013	17.087 ± 0.051	17.184 ± 0.080
2MASS J07474639+2605167	25.35 ± 0.68	25.37 ± 0.56	23.86 ± 0.42	20.68 ± 0.04	18.86 ± 0.03	17.547 ± 0.016	16.679 ± 0.011	16.182 ± 0.020	15.778 ± 0.025
LP 366−18	21.78 ± 0.14	19.49 ± 0.01	18.07 ± 0.01	17.51 ± 0.01	17.17 ± 0.01	16.448 ± 0.008	15.965 ± 0.010	15.531 ± 0.009	15.375 ± 0.012
LHS 1953	20.29 ± 0.04	17.50 ± 0.01	15.93 ± 0.00	15.27 ± 0.00	14.88 ± 0.01	14.106 ± 0.002	13.648 ± 0.010	13.228 ± 0.002	13.027 ± 0.003
LP 366−27	21.79 ± 0.16	19.24 ± 0.01	17.79 ± 0.01	16.46 ± 0.00	15.75 ± 0.01	14.896 ± 0.004	14.376 ± 0.010	13.934 ± 0.004	13.652 ± 0.005
2MASS J08044064+2239502	19.78 ± 0.03	18.28 ± 0.01	17.60 ± 0.01	17.39 ± 0.01	17.31 ± 0.01	16.818 ± 0.011	16.693 ± 0.010	16.832 ± 0.034	17.238 ± 0.072
LP 424−14	20.72 ± 0.06	18.07 ± 0.01	16.62 ± 0.00	15.08 ± 0.00	14.26 ± 0.01	13.332 ± 0.002	12.761 ± 0.010	12.365 ± 0.001	11.997 ± 0.002
ULAS J081045.24+222841.9	25.41 ± 0.72	22.20 ± 0.09	20.28 ± 0.03	18.82 ± 0.01	18.02 ± 0.02	17.189 ± 0.013	16.605 ± 0.010	16.185 ± 0.016	15.952 ± 0.023
ULAS J081127.84+203925.7	22.67 ± 0.56	18.48 ± 0.02	17.49 ± 0.01	17.76 ± 0.02	16.98 ± 0.02	15.999 ± 0.007	15.519 ± 0.010	15.110 ± 0.008	14.908 ± 0.012
LHS 6139	17.77 ± 0.01	15.84 ± 0.00	15.73 ± 0.01	14.25 ± 0.00	13.98 ± 0.00	12.874 ± 0.001	12.448 ± 0.010	11.996 ± 0.001	11.778 ± 0.001
G 40−12	18.15 ± 0.01	15.82 ± 0.00	14.69 ± 0.00	14.83 ± 0.01	13.97 ± 0.00	13.218 ± 0.002	12.812 ± 0.010	12.292 ± 0.001	12.111 ± 0.002
LP 367−56	21.56 ± 0.12	18.81 ± 0.01	17.33 ± 0.01	16.76 ± 0.01	16.40 ± 0.01	15.674 ± 0.005	15.217 ± 0.010	14.776 ± 0.006	14.613 ± 0.008
EGGR 531	17.95 ± 0.01	17.18 ± 0.00	16.84 ± 0.00	16.71 ± 0.00	16.70 ± 0.01	16.168 ± 0.006	15.954 ± 0.010	15.728 ± 0.009	15.665 ± 0.016
ULAS J082155.56+250939.8	–	–	–	–	–	18.610 ± 0.043	17.226 ± 0.015	17.290 ± 0.065	17.232 ± 0.095
LHS 2006	21.78 ± 0.14	18.72 ± 0.01	17.08 ± 0.00	16.08 ± 0.00	15.54 ± 0.01	14.739 ± 0.003	14.254 ± 0.010	13.791 ± 0.003	13.534 ± 0.004
2MASS J08253258+2359306	22.68 ± 0.26	19.79 ± 0.02	18.31 ± 0.01	16.53 ± 0.00	15.59 ± 0.01	14.604 ± 0.003	14.068 ± 0.010	14.14 ± 0.03[a]	13.336 ± 0.004
LP 311−21	21.30 ± 0.10	18.62 ± 0.01	17.15 ± 0.00	16.52 ± 0.00	16.13 ± 0.01	15.359 ± 0.005	14.934 ± 0.010	14.430 ± 0.006	14.210 ± 0.008
2MASS J08332144+2300120	21.95 ± 0.16	19.03 ± 0.01	17.52 ± 0.01	15.80 ± 0.00	14.88 ± 0.01	13.903 ± 0.002	13.359 ± 0.010	12.923 ± 0.002	12.614 ± 0.002
LSPM J0836+2432	20.30 ± 0.05	19.51 ± 0.01	18.90 ± 0.01	18.74 ± 0.01	18.69 ± 0.03	18.197 ± 0.026	17.985 ± 0.028	17.909 ± 0.096	17.968 ± 0.162
LP 321−30	21.93 ± 0.16	19.01 ± 0.01	17.33 ± 0.00	16.44 ± 0.00	15.95 ± 0.01	15.136 ± 0.004	14.643 ± 0.010	14.176 ± 0.004	13.906 ± 0.006
ULAS J085335.33+285902.4	23.16 ± 0.50	24.12 ± 0.43	24.09 ± 0.62	22.17 ± 0.20	20.33 ± 0.13	18.930 ± 0.129	17.705 ± 0.031	16.936 ± 0.123	16.425 ± 0.044
LP 260−3	22.84 ± 0.28	19.81 ± 0.02	18.20 ± 0.01	17.26 ± 0.01	16.69 ± 0.01	15.891 ± 0.006	15.403 ± 0.010	14.931 ± 0.010	14.670 ± 0.012
LP 313−36	21.86 ± 0.13	19.20 ± 0.01	17.61 ± 0.01	16.80 ± 0.01	16.33 ± 0.01	15.537 ± 0.004	15.041 ± 0.010	14.591 ± 0.005	14.323 ± 0.007
WD 0921+315	20.66 ± 0.06	18.73 ± 0.01	17.93 ± 0.01	17.64 ± 0.01	17.50 ± 0.02	16.927 ± 0.009	16.631 ± 0.010	16.408 ± 0.022	16.401 ± 0.038
2MASS J15052821+3115037	23.27 ± 0.42	20.77 ± 0.03	19.09 ± 0.01	17.71 ± 0.01	16.96 ± 0.01	16.131 ± 0.007	15.547 ± 0.010	15.115 ± 0.007	14.810 ± 0.010
LP 272−48	20.91 ± 0.06	18.15 ± 0.01	16.67 ± 0.01	15.35 ± 0.01	14.62 ± 0.01	13.768 ± 0.002	13.239 ± 0.010	12.811 ± 0.002	12.555 ± 0.002
LP 327−24	21.62 ± 0.11	19.18 ± 0.01	17.81 ± 0.01	15.81 ± 0.00	14.63 ± 0.00	13.479 ± 0.002	12.843 ± 0.010	12.259 ± 0.001	11.854 ± 0.001
ULAS J151354.98+303543.9	24.60 ± 0.76	21.44 ± 0.04	20.05 ± 0.02	17.31 ± 0.01	15.79 ± 0.01	14.543 ± 0.003	13.850 ± 0.010	13.343 ± 0.002	12.911 ± 0.002
LHS 3042	23.30 ± 0.42	20.36 ± 0.02	18.72 ± 0.01	16.90 ± 0.01	15.92 ± 0.01	14.973 ± 0.004	14.401 ± 0.010	14.015 ± 0.003	13.697 ± 0.004
LHS 3063	20.25 ± 0.05	18.01 ± 0.01	16.52 ± 0.00	15.03 ± 0.00	14.21 ± 0.00	13.260 ± 0.001	12.763 ± 0.010	12.344 ± 0.001	12.043 ± 0.001
2MASS J15593876+2550362	24.86 ± 0.59	24.38 ± 0.33	23.71 ± 0.30	20.43 ± 0.03	18.57 ± 0.03	17.293 ± 0.017	16.442 ± 0.010	16.099 ± 0.014	15.647 ± 0.018
ULAS J160036.59+284305.7	23.95 ± 0.79	23.82 ± 0.35	23.51 ± 0.38	21.89 ± 0.16	21.49 ± 0.42	18.856 ± 0.060	17.650 ± 0.029	16.833 ± 0.025	16.136 ± 0.031
NLTT 41963	20.42 ± 0.05	18.12 ± 0.01	16.66 ± 0.01	15.17 ± 0.00	14.37 ± 0.01	13.393 ± 0.002	12.897 ± 0.010	12.481 ± 0.001	12.179 ± 0.002
NLTT 42004	22.35 ± 0.17	19.46 ± 0.01	17.83 ± 0.01	16.96 ± 0.01	16.45 ± 0.01	15.596 ± 0.005	15.131 ± 0.010	14.638 ± 0.004	14.406 ± 0.008
NLTT 42650	21.99 ± 0.16	19.85 ± 0.01	18.88 ± 0.01	18.49 ± 0.01	18.33 ± 0.02	17.743 ± 0.022	17.462 ± 0.022	17.355 ± 0.039	17.305 ± 0.083
LP 330−15	24.10 ± 0.76	20.04 ± 0.02	18.39 ± 0.01	17.11 ± 0.01	16.47 ± 0.01	15.579 ± 0.005	15.050 ± 0.010	14.612 ± 0.005	14.312 ± 0.006
LHS 3198	19.73 ± 0.04	17.10 ± 0.00	15.62 ± 0.00	15.06 ± 0.00	14.71 ± 0.00	13.923 ± 0.002	13.498 ± 0.010	13.016 ± 0.002	12.837 ± 0.002
LSPM J1641+3210	23.22 ± 0.38	20.74 ± 0.03	19.22 ± 0.01	16.95 ± 0.01	15.71 ± 0.01	14.642 ± 0.003	14.012 ± 0.010	13.574 ± 0.003	13.223 ± 0.003

[a]No LAS *H*-band data available, 2MASS H magnitude given.

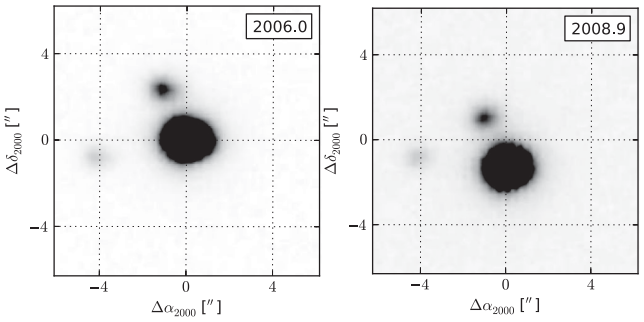

Figure 13. First and second epoch LAS *J* band images of LHS 6139 and ULAS J081127.84+203925.7 centred on the first epoch position of the former. Their common proper motion is evident.

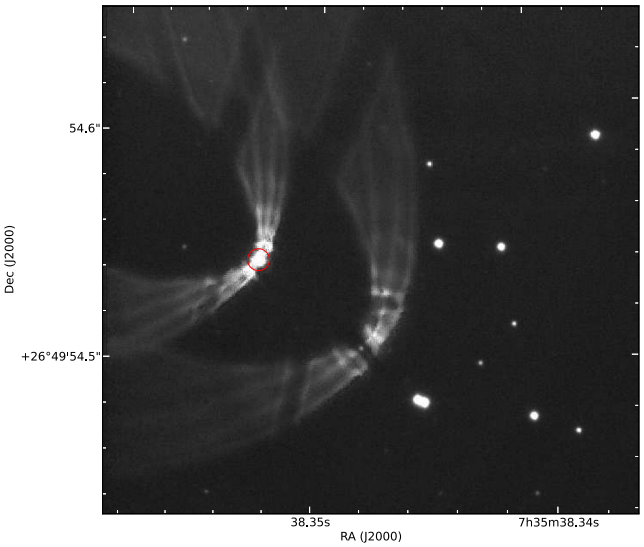

Figure 14. The first epoch *J* band image of the ups Gem ghost source, which has a different position at each epoch giving a false high proper motion. The source is indicated by the red circle.

the reader to Catalán et al. (2012) for a description of the ultracool H rich white dwarf LSR J0745+2627 which was identified due to its unusually high proper motion in an early version of this catalogue and subsequent photometric analysis and spectroscopic confirmation.

5.3 L dwarfs

Several hundred L dwarfs have been identified in the local field by wide field surveys, e.g. Kirkpatrick et al.(1999, 2008). Detection of new L dwarfs remains valuable because only a few have been identified that are in age-benchmark binaries (e.g. Zhang et al. 2010) which can be used to test model atmospheres. Similarly, a very small proportion of L dwarfs have high space motions and unusually red or unusually blue $(J - K)$ colours (see e.g. Kirkpatrick et al. 2010, and references therein). Some of these are sub-L dwarfs with low metallicity and halo kinematics ($v_{\rm tan} = 200$–320 km s^{-1}; Schilbach, Röser & Scholz 2009). More detections of such rare types of L dwarf are needed to better understand the population as a whole, and it is reasonable to expect that a large proper motion survey such as this may find some examples.

We present here the initial results of a search of the UKIDSS DR8 subset of our proper motion catalogue in order to illustrate the practicality of future searches. The DR8 subset comprises 260 deg^2 of our catalogue. We first selected sources whose proper motions have $\geq 5\sigma$ significance, $(Y-J) > 0.7$ and $(J - H) > 0.6$. This first colour selection will include many late M dwarfs, but it will include nearly all L dwarfs. 137 candidates were identified, all of which also satisfy the following UKIDSS quality criteria: merged class $= -1$ (i.e. a stellar image profile), ellipticity < 0.3 in both *J* band images and ppErrBits<256 in both *J* band images. We then used the optical data from SDSS DR8 to refine the selection. Hawley et al. (2002) presented the average $(r - i)$, $(i - z)$, $(z - J)$ and $(i - J)$ colours for objects of spectral types M0 to T6 that were identified in SDSS. The plots shown in fig. 8 of that work demonstrate that the $(i - J)$ colour is best for spectrophotometric typing, and in particular for distinguishing M dwarfs from L dwarfs, so we used this colour to define our final sample. Their *J* band data were presented on the 2MASS system, so we put them on the MKO system before making a colour cut, which was $(i - J) \geq 4.4$. Only 21 objects remained, all of which passed visual inspection for defects and blending. All of these 21 also have $i - z > 1.8$ and they are drop outs in the *u* and *g* passbands, these properties are consistent with L dwarf status. They are listed in Table 3.

In Fig. 15, we plot the proper motion against $(i - J)$ colour (left-hand panel) and the reduced proper motion, H_J, against $(i - J)$ colour. There is a trend for the reddest objects to have the largest reduced proper motions as would be expected if the reddest objects tend to be the coolest and least luminous.

A search of the SIMBAD data base shows that 6 of these 21 L dwarf candidates are known in the literature: 5 are known L dwarfs and one, ULAS J154432.76+265551.6, is an L dwarf photometric candidate previously identified using SDSS and UKIDSS photometry (Zhang et al. 2009). The absence of late M dwarfs indicates that our selection has been successful, despite the significant scatter in the colours of late M and L dwarfs, and the larger volume probed for earlier types in a magnitude-limited sample (limited by the sensitivity of UKIDSS and SDSS in this case). Of the five known L dwarfs in Table 3, ULAS J092933.50+342952.1 is type L8 (Kirkpatrick 2000), ULAS J163352.78+305223.1 is type L2 (Zhang et al. 2010), ULAS J164522.04+300406.8 is type L3 (Cruz et al. 2007), ULAS J075656.40+231456.6 is type L3.5 and ULAS J161626.46+221859.4 is type L5 (both from Knapp et al. 2004). A comparison between these spectral types and spectrophotometric types that we inferred from the $(i - J)$ colour showed agreement to within 1 or 2 subtypes in 4 out of 5 cases, so we list spectrophotometric types for the 21 L dwarf candidates in the table, quoting only limits for objects with photometric uncertainty >0.3 mag in the *i* magnitude.

5.4 T dwarfs

Burningham et al. (2013) present proper motions from our catalogue for 128 UKIDSS T dwarfs, including two new benchmark T dwarfs LHS 6176B and HD 118865B.

We also investigated the characteristic population age of late T dwarfs (Smith et al. 2013) in response to current atmospheric models suggesting they are young and low mass (Leggett et al. 2009, 2010, 2012). For this, we used tangential velocity data calculated using proper motions from this and other catalogues and spectrophotometric distances where parallax data were unavailable (Marocco et al. 2010; Andrei et al. 2011; Dupuy & Liu 2012; Kirkpatrick et al. 2012). We concluded that the kinematic age of the population

Table 3. L dwarf candidates identified in the LAS DR8 area. Proper motion values are in units of mas yr^{-1}. Near-infrared photometry is UKIDSS LAS DR8, *J* band is first epoch. Optical photometry is SDSS DR8.

Name	$\mu_\alpha \cos\delta$	μ_δ	J	$J-H$	$H-K$	$i-J$	$i-z$	Estimated type	Actual type
ULAS J073933.51+230709.4	-84 ± 14	-122 ± 14	18.143	0.82	0.68	6.14	3.3	>L7	
ULAS J075656.40+231456.6	162 ± 10	-154 ± 10	16.958	1.14	0.83	5.95	3.17	>L7	L3.5[a]
ULAS J080441.08+182611.8	-145 ± 9	-65 ± 7	17.545	1.03	0.71	5.72	3.26	>L6	
ULAS J083023.24+235538.6	89 ± 7	-123 ± 7	17.418	1.16	0.77	5.64	3.09	>L6	
ULAS J092933.50+342952.1	-231 ± 13	-80 ± 11	16.743	1.08	0.88	5.64	2.74	L6	L8[b]
ULAS J093336.29+333701.9	-23 ± 9	-221 ± 10	17.154	0.66	0.72	4.46	1.97	L0	
ULAS J145949.58+330125.1	83 ± 9	-95 ± 10	16.702	0.61	0.55	4.57	2.16	L1	
ULAS J150231.71+312056.5	-10 ± 11	-88 ± 10	17.911	0.84	0.61	4.48	2.38	L0	
ULAS J152225.03+304917.2	-35 ± 10	-61 ± 9	18.043	0.77	0.67	4.58	2.74	L1	
ULAS J153158.93+282954.7	-79 ± 12	25 ± 12	18.517	0.63	0.02	4.44	2.29	>L0	
ULAS J154432.76+265551.6	-87 ± 11	95 ± 15	16.223	0.92	0.78	5.09	2.22	L3	
ULAS J161626.46+221859.4	-51 ± 7	25 ± 6	17.462	1.06	0.77	5.58	2.87	>L6	L5[a]
ULAS J162052.30+275115.7	10 ± 12	-145 ± 10	17.609	0.85	0.68	4.85	2.27	L2	
ULAS J162339.03+253511.3	-152 ± 6	1 ± 5	17.121	1.12	0.84	5.12	1.95	L3	
ULAS J163352.78+305223.1	-25 ± 9	-113 ± 8	16.626	0.74	0.62	4.53	1.96	L1	L2[c]
ULAS J163713.53+303808.4	-142 ± 9	54 ± 6	17.375	0.71	0.51	4.90	1.93	L3	
ULAS J163836.80+281003.0	18 ± 6	-111 ± 7	17.067	0.65	0.58	4.45	1.82	L0	
ULAS J164131.57+282015.8	-30 ± 5	64 ± 8	17.018	0.93	0.8	4.58	1.7	L1	
ULAS J164301.34+322407.2	-54 ± 7	121 ± 10	16.385	0.61	0.48	4.62	2.08	L1	
ULAS J164456.00+311228.8	-6 ± 7	-133 ± 6	16.538	0.65	0.55	4.41	2.08	L0	
ULAS J164522.04+300406.8	-74 ± 3	-67 ± 8	15.08	0.85	0.71	4.69	1.81	L2	L3[d]

[a]Knapp et al. (2004).
[b]Kirkpatrick (2000).
[c]Zhang et al. (2010).
[d]Cruz et al. (2007).

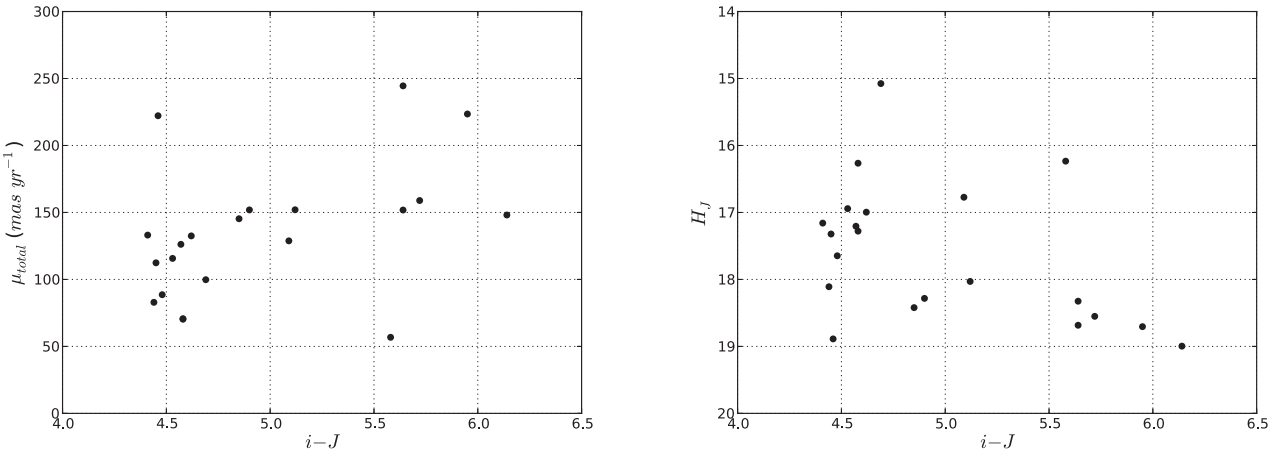

Figure 15. $i-J$ colour versus total proper motion (*left*) and *J* band reduced proper motion (*right*) for the 21 L dwarfs presented in Table 3.

is older than that predicted by the models and, ultimately, more benchmarks are needed to anchor them.

Pinfield et al. (2012) presented a proper motion for the T8.5 dwarf WISEP J075003.84+272544.8 from a prototype version of our catalogue. We note that WISEP J075003.84+272544.8 was independently identified by us in a search for T dwarfs with high reduced proper motions shortly before its publication by the *WISE* team. We now provide the most up to date proper motion from this final revision of our catalogue of -736 ± 13 and -195 ± 15 mas yr^{-1} in $\mu_\alpha \cos\delta$ and μ_δ, respectively (the uncertainty is reduced and the proper motion difference is within the uncertainties).

Comparison of our new measured proper motion for the halo T dwarf candidate ULAS J1319+1209 with that reported in Murray et al. (2011) highlights a significant discrepancy. We measure a considerably lower proper motion, which suggests kinematics most consistent with membership of the Galactic disc, rather than the halo. The previous measurement by Murray et al. (2011) appears to be in error, with the likely source a dramatic underestimate of the uncertainty in the centroid in its second epoch imaging combined with a relatively short epoch baseline between the observations. Our new measurement benefits from considerably higher precision thanks to deeper UKIDSS second epoch imaging, and a ∼5 year epoch baseline, compared to 0.8 years in the Murray et al. (2011) case.

Results of searches for new T dwarfs with large proper motions, including the identification of two candidate thick disc/halo members, will be reported in a future publication.

5.5 Brown dwarf benchmark searches

We undertook various searches for benchmark UCDs, the parameters of which and known objects recovered are shown here. Given that parameters derived from atmospheric models of UCDs are uncertain it is helpful to constrain them through associations with objects in a common system (Pinfield et al. 2006). See Section 6 for results.

L dwarfs in DR8

We performed a search for binary companions to the 21 L dwarf candidates presented in Section 5.3 by cross-matching against the optical proper motion catalogue of Munn et al. (2004), which has higher precision than the UKIDSS LAS catalogue, owing to the much longer time baseline. A cross-match radius of 1000 arcsec was used, which is sufficient to detect candidates within 20 000 au in every case, even if a 'near' distance corresponding to spectral type L9 is assumed for each candidate. We found 61 sources as possible companions to three sources from Table 3 that have proper motion vectors consistent to within 2σ. (This was defined by computing the difference between the L dwarf's UKIDSS proper motion vector and the companion star's Munn catalogue proper motion vector and determining whether the length of the resulting vector is consistent with zero, to within 2σ). Of these 61 possible companions, 22 are listed as non-stellar sources in UKIDSS (i.e. the parameter *pstar <0.5*) usually indicating an extended source. We estimated spectrophotometric types and distances to the remaining 39 sources using their SDSS fluxes and the data of Finlator et al. (2000) and West et al. (2011) and found that every candidate was ruled out either because its heliocentric distance was far too great to be a companion to the L dwarf, or because the projected separation at the distance of the star was >50 000 au.

We also searched for binary companions via an internal match of the UKIDSS LAS proper motion catalogue, in order to detect any companions that might be too faint to appear in the Munn catalogue. We searched only within a 300 arcsec radius, since binaries with cool primaries (M type or later) have not yet been found with separations >6000 au. We using the same criterion that the proper motion vectors agree to within 2σ and the companion must have *pstar* > 0.5, and an additional criterion that the candidate companion must have a brighter J magnitude than the L dwarf. We found six candidates, only one of which (a star with mid-M-type colours) had not been detected and ruled out in the previous match against the Munn catalogue. This object is too distant to be a companion to the L dwarf. We therefore conclude that none of the 21 L dwarf candidates have stellar companions.

L and early T dwarfs in the full survey

We searched the full 1500 deg^2 of data for new L and T candidates, in particular new benchmark objects, we selected sources with $Y - J > 0.8$ that were also classified as stellar in both J band images and fell into one or more of the following groups.

No H band detection, stellar merged class and proper motion > 350 mas yr^{-1} (21 sources);

$J - H > 0.8$, and proper motion >500 mas yr^{-1} (6 sources);

$J - K > 1.4$, and proper motion >500 mas yr^{-1} (17 sources);

$J - H > 0.6$, $H - K > 0.5$ and proper motion >500 mas yr^{-1} (12 sources).

There were a further 21 sources with $Y - J > 0.8$ and proper motion >500 mas yr^{-1} that did not meet the other near-infrared colour cuts, we elected to take a closer look at these as well since there were relatively few and sources with such large proper motions are often interesting in some way. These groups, taking into account sources in multiple groups, make 57 sources for further study.

We matched to the UKIDSS late T dwarf catalogue maintained by Ben Burningham and we found nine matches with spectral types ranging from T5 to T9. We also matched to SIMBAD and find a further seven L dwarfs (including one listed as an L dwarf candidate). This demonstrates the efficacy of our brown dwarf selection criteria.

We searched for benchmark candidates within our sample by retrieving a list of stars with proper motions greater than 350 mas yr^{-1} from SIMBAD and cross-matching with our list of 57 brown dwarf candidates within 5 arcmin and with proper motion difference tolerances of 50 mas yr^{-1} independently in RA and Dec. Four potential benchmark objects have separations ranging from 64 to 111 arcsec. G 62−33/2MASS J13204427+0409045 are a known K2/L3 binary (Faherty et al. 2010). Ross 458A/C (Goldman et al. 2010; Burningham et al. 2011) and GJ 576/WISEP J150457.58+053800.1 (Scholz 2010; Murray et al. 2011) are also recovered. The fourth candidate is found to be cross-talk from the bright potential primary upon further inspection of the images. Interestingly, the bright star from which our fourth candidate is cross-talk is itself the fainter component of a common proper motion group, the primary being LHS 2968.

Extended red search

In Section 4.5, we found 834 red (Y-J > 0.7) sources with genuine large motions between the observation epochs (>500 mas). This translates to genuine proper motions down to around 75 mas yr^{-1}. Note that this selection also incorporates most of the objects selected in Section 5.5.2. Within this sample, we identified 33 sources with a possible common proper motion companion within the 1 arcmin × 1 arcmin image.

In an attempt to recover common proper motion companions to these interesting sources we looked within our catalogue for nearby objects (1 arcmin radius) with proper motion differences within 1σ significance. In practice, we found 1σ to be sufficient since matches above that were typically of the order of 5σ or greater. We recovered 13 matches meeting these criteria which produced 12 common proper motion pairs since two of the matches were both components of the same pair. We find that four of these are known common proper motion pairs according to SIMBAD. The 12 pairs are shown in Section 6, Table 4.

To expand our candidate brown dwarf binary list to include pairs with a primary too bright to be included in our catalogue, we used a list of SIMBAD objects with proper motions greater than 100 mas yr^{-1}. We looked for companions to the 834 red sources with genuine large motions within 10 arcmin and with $\mu_\alpha \cos\delta$ and μ_δ differences less than 30 mas yr^{-1} independently of one another. We found 175 matches to these criteria, though we expected many to have been matched to themselves. In order to remove the self-matches from our candidate list we rejected those with separation < 5 arcsec or J magnitude difference <0.5, which should leave only genuine pairs, variable sources, or those with very high proper motion. 31 candidate pairs survived this cut. Of these we found five pairs had been identified in our internal search and two high proper motion single stars had survived the previous cut, leaving 24 systems (see Section 6, Table 5).

Table 4. The 12 common proper motion systems identified within the catalogue from Section 5.5.3.

α	δ	i	z	J	H	K	$\mu_\alpha \cos\delta$ (mas yr^{-1})	μ_δ (mas yr^{-1})	$i-J$	SIMBAD entry	Spectral type	Known binary
09:53:24.13	+05:27:01.3	15.64 ± 0.00	14.68 ± 0.00	13.13 ± 0.01	12.58 ± 0.00	12.24 ± 0.00	−185 ± 8	38 ± 7	2.51	y	M4	[b]
09:53:24.45	+05:26:58.7	20.20 ± 0.04	18.21 ± 0.02	15.74 ± 0.01	15.05 ± 0.01	14.47 ± 0.01	−188 ± 9	39 ± 6	4.46	y	M9.5	
09:56:14.81	+01:44:57.5	14.12 ± 0.00	13.49 ± 0.00	12.11 ± 0.01	11.65 ± 0.00	11.40 ± 0.00	−105 ± 11	−182 ± 9	2.01	y	M2	[b]
09:56:13.07	+01:45:13.1	20.29 ± 0.04	18.50 ± 0.04	16.35 ± 0.01	15.92 ± 0.01	15.48 ± 0.02	−109 ± 11	−177 ± 9	3.94	y	M9	
11:58:25.59	−01:22:58.9	15.34 ± 0.00	14.49 ± 0.00	12.95 ± 0.01	12.49 ± 0.00	12.18 ± 0.00	−201 ± 8	−74 ± 7	2.39	y	*M4*[a]	
11:58:24.04	−01:22:45.5	20.31 ± 0.04	18.69 ± 0.04	16.64 ± 0.01	16.12 ± 0.01	15.66 ± 0.02	−208 ± 10	−75 ± 7	3.67	y	M8	
11:59:48.15	+07:06:59.1	18.49 ± 0.01	17.16 ± 0.01	15.30 ± 0.01	14.80 ± 0.01	14.40 ± 0.01	−160 ± 12	101 ± 10	3.19	y	M7	[c]
11:59:48.47	+07:07:09.1	17.81 ± 0.01	18.01 ± 0.02	17.52 ± 0.04	17.58 ± 0.06	17.49 ± 0.10	−159 ± 12	102 ± 10	0.29	y	WD?	
12:08:16.83	+08:45:27.6	17.67 ± 0.01	16.08 ± 0.01	13.94 ± 0.01	13.37 ± 0.00	12.90 ± 0.00	−122 ± 7	−68 ± 9	3.73	y	M9	
12:08:15.55	+08:45:42.7	17.77 ± 0.01	17.64 ± 0.01	16.75 ± 0.02	16.51 ± 0.02	16.40 ± 0.03	−123 ± 8	−66 ± 9	1.02	y	WD	
13:25:13.86	+12:30:13.3	17.96 ± 0.01	16.85 ± 0.01	15.11 ± 0.01	14.56 ± 0.00	14.21 ± 0.01	−95 ± 8	−41 ± 8	2.85	n	*M5/6*[a]	
13:25:12.44	+12:30:22.0	20.37 ± 0.04	18.70 ± 0.04	16.42 ± 0.01	15.79 ± 0.01	15.31 ± 0.01	−98 ± 8	−38 ± 8	3.95	n	*M8.5/9*[a]	
13:28:35.49	+08:08:19.5	18.34 ± 0.01	17.06 ± 0.01	15.27 ± 0.01	14.74 ± 0.01	14.35 ± 0.01	−145 ± 8	−60 ± 9	3.07	n	*M6*[a]	
13:28:34.69	+08:08:18.9	20.52 ± 0.04	18.62 ± 0.03	16.45 ± 0.01	15.86 ± 0.01	15.33 ± 0.01	−145 ± 8	−60 ± 9	4.07	y	M8.5	
14:04:40.20	−00:40:19.8	15.52 ± 0.00	14.63 ± 0.00	13.06 ± 0.01	12.56 ± 0.00	12.24 ± 0.00	−135 ± 8	−79 ± 10	2.46	n	*M4*[a]	
14:04:40.39	−00:40:26.9	17.17 ± 0.01	16.03 ± 0.01	14.25 ± 0.01	13.72 ± 0.00	13.35 ± 0.00	−136 ± 8	−81 ± 10	2.92	n	*M6*[a]	
14:20:16.86	+12:07:38.9	16.18 ± 0.00	15.21 ± 0.01	13.55 ± 0.01	13.09 ± 0.00	12.71 ± 0.00	−108 ± 7	−21 ± 8	2.64	n	*M5*[a]	
14:20:17.83	+12:07:53.5	20.76 ± 0.07	18.86 ± 0.05	16.54 ± 0.01	15.89 ± 0.01	15.35 ± 0.01	−113 ± 8	−20 ± 8	4.22	n	*L0*[a]	
14:24:38.98	+09:17:09.4	20.53 ± 0.06	18.46 ± 0.03	15.68 ± 0.01	14.80 ± 0.00	14.07 ± 0.00	−221 ± 7	−156 ± 4	4.85	y	L4	[d]
14:24:39.04	+09:17:13.1	14.91 ± 0.01	14.89 ± 0.01	14.52 ± 0.01	14.52 ± 0.00	14.58 ± 0.01	−211 ± 7	−156 ± 4	0.39	y	DA	
14:59:41.64	+08:35:07.7	18.69 ± 0.01	17.63 ± 0.02	15.83 ± 0.01	15.31 ± 0.01	14.98 ± 0.01	43 ± 7	−85 ± 5	2.86	n	*M5/6*[a]	
14:59:41.92	+08:35:13.5	20.28 ± 0.04	19.13 ± 0.05	17.18 ± 0.02	16.71 ± 0.04	16.37 ± 0.04	50 ± 6	−85 ± 5	3.10	n	*M6*[a]	
15:49:51.57	+08:57:29.6	15.45 ± 0.00	14.70 ± 0.00	13.20 ± 0.01	12.68 ± 0.00	12.40 ± 0.00	−55 ± 3	−100 ± 5	2.25	n	*M4*[a]	
15:49:51.88	+08:57:30.7	20.03 ± 0.03	18.50 ± 0.03	16.29 ± 0.01	15.76 ± 0.01	15.28 ± 0.01	−57 ± 4	−101 ± 5	3.74	n	*M8*[a]	

[a]Indicates an estimated spectral type based on $i-J$ colour using Hawley et al. (2002) as in Section 5.3.
[b]Zhang et al. (2010).
[c]Deacon et al. (2009).
[d]Becklin & Zuckerman (1988).

Table 5. The 24 probable common proper motion systems identified in conjunction with SIMBAD from Section 5.5.3.

Primary name	Spectral type	Secondary α	δ	J	$\mu_\alpha \cos\delta$ (mas yr^{-1})	μ_δ (mas yr^{-1})	$i-J$	Spectral type	Pair Separation (arcsec)	$\mu_{\rm diff}$ σ	Known binary
NLTT 21820		09:27:53.47	+01:49:13.9	17.95 ± 0.03	-26 ± 8	-138 ± 8	3.17 ± 0.10	*M6*[a]	111	1.7	
LP 488−31		09:46:12.09	+11:16:31.0	15.66 ± 0.01	-187 ± 6	-25 ± 6	3.33 ± 0.01	*M7*[a]	10	0.5	[b]
2MASS J10084007+0150537		10:09:04.17	+01:58:46.5	17.99 ± 0.05	34 ± 7	-163 ± 10	> 3.3	$>$ *M6.5*[a]	595	1.5	
2MASS J12020964+0742538		12:01:59.65	+07:35:53.6	14.97 ± 0.01	127 ± 7	-136 ± 7	3.69 ± 0.01	M8	446	1.4	
2MASS J12020933+0742477		12:01:59.65	+07:35:53.6	14.97 ± 0.01	127 ± 7	-136 ± 7	3.69 ± 0.01	M8	438	1.4	
SDSS J120331.33−005332.8		12:02:53.30	−00:56:08.3	15.87 ± 0.01	-216 ± 5	-22 ± 4	4.05 ± 0.03	*M9*[a]	591	3.3	
10 Vir	K3III	12:09:49.00	+01:52:38.3	14.65 ± 0.01	57 ± 8	-192 ± 4	3.32 ± 0.01	*M7*[a]	137	2.2	
DT Vir	M2Ve	13:00:41.73	+12:21:14.7	16.68 ± 0.01	-639 ± 9	-24 ± 10	6.60 ± 0.57	T8.5	105	1.8	[c]
HD 115151	G5	13:15:13.10	+10:41:57.6	15.85 ± 0.01	-154 ± 7	-20 ± 6	3.64 ± 0.02	*M8*[a]	39	0.7	
G 63−23	K5	13:20:41.49	+09:57:49.7	13.65 ± 0.01	-251 ± 8	-142 ± 6	3.81 ± 0.01	M8	169	0.1	[d]
LHS 2722	K2V	13:20:43.97	+04:09:06.4	15.18 ± 0.01	-498 ± 9	199 ± 10	4.71 ± 0.03	L3	68	0.8	[d]
2MASS J13272850+0916323		13:27:26.77	+09:16:05.6	14.52 ± 0.01	-143 ± 5	-67 ± 4	3.43 ± 0.01	*M7*[a]	37	0.3	[b]
2MASS J13284331+0758378		13:28:34.69	+08:08:18.9	16.45 ± 0.01	-145 ± 8	-60 ± 9	4.07 ± 0.04	M8.5	595	1.3	
2MASS J13284331+0758378		13:28:35.49	+08:08:19.5	15.27 ± 0.01	-145 ± 8	-60 ± 9	3.07 ± 0.01	*M6*[a]	593	1.3	
BD+13 2724	G5	13:54:41.14	+12:47:47.5	18.29 ± 0.05	-103 ± 9	10 ± 11	3.68 ± 0.15	*M8*[a]	574	1.3	
LHS 2875	M2.5	14:12:11.72	−00:35:14.3	13.03 ± 0.01	-705 ± 8	221 ± 6	3.63 ± 0.01	M6	14	1.1	[e]
2MASS J14493646+0533379		14:49:46.20	+05:36:53.4	17.79 ± 0.04	-107 ± 10	-135 ± 10	4.35 ± 0.39	*L1*[a]	243	1.0	
2MASS J14511622+0922464		14:51:24.61	+09:20:05.0	14.35 ± 0.01	-156 ± 5	-33 ± 4	3.28 ± 0.01	*M6.5*[a]	204	1.3	
G 66−40		14:54:08.08	+00:53:25.6	15.07 ± 0.01	-270 ± 9	35 ± 9	3.84 ± 0.01	*M8.5*[a]	23	0.3	
2MASS J14552241+0419361		14:55:23.27	+04:19:48.6	16.12 ± 0.01	-137 ± 11	-39 ± 10	3.24 ± 0.02	*M6.5*[a]	18	1.4	
USNO-B1.0 0988−00251407		14:59:35.25	+08:57:51.2	17.92 ± 0.03	-172 ± 10	-83 ± 7	> 3.4	T4.5	386	1.4	[f]
LHS 3020	K8V	15:04:57.66	+05:38:00.8	16.59 ± 0.02	-616 ± 11	-523 ± 9	7.26 ± 0.51	T6.5	64	1.4	[c]
G 151−59	K0	15:25:57.45	−02:04:56.4	17.85 ± 0.05	179 ± 9	-158 ± 10	4.43 ± 0.16	*L1*[a]	46	0.6	
TYC 2032-546-1		15:32:52.33	+28:51:28.5	18.39 ± 0.06	-142 ± 9	-131 ± 9	> 2.9	$>$ *M6*[a]	10	1.5	

[a]Indicates an estimated spectral type based on $i-J$ colour using Hawley et al. (2002) as in Section 5.3.
[b]Deacon et al. (2009).
[c]Scholz (2010).
[d]Faherty et al. (2010).
[e]Luyten (1979a).
[f]Day-Jones et al. (2011).

6 NEW CANDIDATE BENCHMARKS

Amongst the 36 sources in Tables 4 and 5 there are 29 ultracool benchmark binary candidates, of which 15 are new and survive a test for common distance. Below we discuss those for which the primary has a distance in the literature and rule out three candidates. All of the remainder have spectrophotometric distances consistent with binarity (see Tables 6 and 7). Note that unless stated otherwise

Table 6. Upper and lower distance estimates for the components of the new binary candidates in Table 4. Distances are calculated using LAS first epoch *J* band magnitude and absolute J magnitudes from Dupuy & Liu (2012) (≥M6) and Hawley et al. (2002) (<M6) and the spectral types in Table 4 ± 1 subtype where they are $i - J$ based estimates. Note that we find the SDSS and UKIDSS photometry of the secondary component of 1208+0845 fits that of an ∼5000 K H-rich white dwarf, we have used this to produce our distance estimate in this case.

α a	δ a	d_{min} a pc	d_{max} a pc	d_{min} b pc	d_{max} b pc
11:58:25.59	−01:22:58.9	50	139	130	130
14:04:40.20	−00:40:19.8	53	146	53	91
15:49:51.57	+08:57:29.6	56	155	99	134
14:20:16.86	+12:07:38.9	55	110	89	111
12:08:16.83	+08:45:27.6	34	34	41	41
13:25:13.86	+12:30:13.3	78	226	96	121
13:28:35.49	+08:08:19.5	84	146	105	105
14:59:41.64	+08:35:07.7	109	314	203	354

Table 7. Upper and lower distance estimates for the components of the unknown binary candidates in Table 5. Distances to the primaries are calculated using fits of available photometry (B/V, J, H, K) to atmospheric models of main-sequence stars. Missing values in the χ^2 column indicate that we were unable to fit an $T_{\rm eff}$ to the photometry or the photometry was unavailable. The results of solutions with a χ^2 value greater than 10 are not included as we deem them too unreliable. Upper and lower limits of ± 50 per cent are used to take into account photometric scatter and other sources of uncertainty. Note that our distance estimates calculated in this way are consistent with parallax based distances where available. Distance estimates to the secondary components are calculated using the same method as that in Table 6. The only binary candidate we are able to rule out with confidence is BD+13 2724.

Name a	d_{min} a pc	d_{max} a pc	χ^2 a	d_{min} b pc	d_{max} b pc
NLTT 21820	272	817	9.95	289	416
2MASS J14493646+0533379			193.82	137	179
2MASS J12020964+0742538				61	61
2MASS J12020933+0742477				61	61
TYC 2032-546-1	119	357	0.28	13	508
SDSS J120331.33−005332.8				74	92
2MASS J10084007+0150537			23.9	11	323
2MASS J13284331+0758378				106	106
G 151−59	45	136	0.31	118	185
G 66−40	32	96	9.25	56	63
2MASS J13284331+0758378				84	121
LP 488−31	61	182	1.49	83	144
2MASS J13272850+0916323	38	115	3.55	49	86
HD 115151	42	127	0.76	81	109
BD+13 2724	40	120	0.0	248	337
2MASS J14511622+0922464			22.18	55	79
10 Vir				52	91
2MASS J14552241+0419361	63	189	4.27	124	178

Y, *J*, *H* and *K* magnitudes in this section are on the MKO system and *J* band photometry is UKIDSS first epoch.

G 151−59

G 151−59 has a *Hipparcos* parallax of 12.63 ± 2.21 mas, placing it at a distance of between 67 and 96 pc. Being relatively bright (2MASS J = 8.98 ± 0.03) it is a well-studied K0 type dwarf with known radial velocity (16.98 ± 0.20 km s^{-1}; Latham et al. 2002) and approximately solar metallicity. If we assume this to be a genuine common proper motion pair then the secondary (ULAS J152557.45−020456.4, $J = 17.85 \pm 0.05$) must be of type L4 to L6 to place it within the same distance range using the Dupuy & Liu (2012) spectral type to absolute J magnitude relations. Despite the estimated type of L1 given in Table 5 this is not ruled out as a genuine pair given the inherent uncertainty in $i - J$ based spectral types of early to mid-L dwarfs. To assess whether G 151−59 and the candidate companion might be a chance projection of two objects at different distances, we loosely followed the method used by Gomes et al. (2013). We calculated distances for early L dwarfs (L0–L4) using the LAS J magnitude of our candidate and the spectral type to absolute J magnitude (MKO) relations of Dupuy & Liu (2012). We then calculated the expected numbers of such L dwarfs in the volume between ±23 per cent of each distance and a 46 arcsec angular radius using the early L dwarf density of 0.0019 pc^{-3} provided by Cruz et al. (2003) and the breakdown amongst subtypes provided by fig. 12 of that work. The ±23 per cent distance range is based on the typical spread of 0.3 mag in the absolute J magnitudes (approximately 15 per cent of the distance) of early L dwarfs added in quadrature to the 17.5 per cent uncertainty in the distance to G 151−59. We expect to find 4×10^{-4} early L dwarfs. It is therefore clearly improbable that our candidate is present simply due to a chance alignment. When the significance of the proper motion similarity with G 151−59 is also taken into account the chance is lower still. Assuming the candidate is a genuine companion, we calculate a tangential velocity between 75 and 108 km s^{-1} when the range of possible *Hipparcos* distances is taken into account. Note that a distance compatible with an L0 dwarf would imply a tangential velocity of the order of 200 kms^{-1}, which is larger than that of the normal disc population. At the distance range of the potential primary, the pair would have a physical separation of between 3100 and 4400 au.

10 Vir

10 Vir (BD+02 2517A) has a *Hipparcos* parallax of 13.69 ± 0.31 mas corresponding to a distance of between 71 and 75 pc and an USNO-B *I* magnitude of 4.7. Assuming this is a genuine common proper motion pair then the secondary must be of type M5 to M8, using the spectral type to MKO absolute J magnitude relation of Dupuy & Liu (2012), taking into account the uncertainties on the spectral types of those within this range of fig. 25 in that work, and its UKIDSS J magnitude of 14.65 ± 0.01. This spectral type range is consistent with the estimate given in Table 5, we therefore conclude this to be a likely common proper motion companion. 10 Vir has one known close companion, BD+02 2517B (Mason et al. 2001) though we are unable to recover this object in our catalogue. Mason et al. (2001) give a V magnitude of 13.4 for BD+02 2517B which should be easily visible in the UKIDSS *J* band image, though we find no source at the given position. This may be explained by the 1909 observation epoch and large proper motion. On inspection

of the two epochs of UKIDSS *J* band images it is apparent that there is a close (4.5 arcsec separate) common proper motion companion to 10 Vir. This source is not detected in UKIDSS *Y, J* and *H* bands due to the close proximity of 10 Vir, the *K* band detection (magnitude 12.425 ± 0.002) may be contaminated by a diffraction spike. If we are to assume that this is BD+02 2517B then we provide an updated position of 12:09:41.73+01:53:45.28 at the UKIDSS *K* band epoch of 2008-05-28. We therefore conclude that our late M dwarf common proper motion companion is a likely third, widely separated (10 000 au) component of this system.

HD 115151

HD 115151 has a *Hipparcos* parallax of 10.73 ± 1.16 mas corresponding to a distance of between 84 and 104 pc and a 2MASS J magnitude of 7.87 ± 0.03. Assuming this is a genuine common proper motion pair then the secondary must be of type M6 to L1, using the spectral type to MKO absolute J magnitude relation of Dupuy & Liu (2012), taking into account the uncertainties on the spectral types of those within this range of fig. 25 in that work and its UKIDSS J magnitude of 15.85 ± 0.01. This spectral type range is consistent with the estimate given in Table 5, we therefore conclude this to be a likely binary.

LP 488−31 and 2MASS J13272850+0916323

These binaries are identified in table 3 of Deacon et al. (2009) but not commented further upon.

BD+13 2724

The BD+13 2724 binary companion does not have a distance estimate compatible with that of the primary (see Table 7), we therefore rule out these two sources as being part of a common system.

SDSS J120331.33−005332.8

SDSS J120331.33−005332.8 is a G type subdwarf with a heliocentric distance of 378 ± 35 pc (Dierickx et al. 2010). This pair has a weak proper motion match and the candidate secondary, a late M dwarf, would be within 100 pc so we have ruled this out as a binary pair.

2MASS J13284331+0758378

2MASS J13284331+0758378 is at first glance a widely separated (10 arcmin) proper motion match to the M8.5/M6 candidate binary pair in Table 4. When the Zhang et al. (2010) distance estimate of 118 pc for the M8.5 dwarf in that system is adopted, the physical separation of that system and 2MASS J13284331+0758378 works out at 70 000 au. 2MASS J13284331+0758378 is likely to be an M7/8 dwarf based on its $i - J$ colour and its distance is therefore incompatible with the M6/M8.6 internal binary pair and we can safely rule it out as a third component.

7 CONCLUSION

We present our UKIDSS LAS derived proper motion catalogue for approximately 1500 deg^2 of northern sky. Proper motions range from 0 to our hard proper motion detection limit of 3.3 arcsec yr^{-1} with a typical 1σ uncertainties of about 10 mas yr^{-1} for bright sources (see Fig. 5).

We find proper motions to be largely reliable for sources brighter than about magnitude 19 in the *J* band, with low ellipticity and stellar morphological classification. While the reliability diminishes we are still finding genuine high proper motions at objects fainter than $J = 19$. Correlation of proper motions with existing optical catalogues is good, although we note that a small percentage (0.5 per cent) of motions are measured using deprecated frames and their accuracy suffers as a result.

The catalogue has already enabled the identification of a variety of high proper motion sources in particular LSR J0745+2627, WISEP J075003.84+272544.8 and two T dwarf benchmarks: LHS 6176B and HD 118865B. In addition, we identify 15 new candidate benchmark UCDs which significantly increase the sample of benchmarks. We are continuing to mine the catalogue for interesting objects and pursuing our own science goals. We would now like to invite the wider community to join us.

ACKNOWLEDGEMENTS

We would like to thank the referee, Hugh C. Harris, for a helpful report. This research was funded in part by the Science and Technology Facilities Council (STFC). This work is based in part on data obtained as part of the UKIRT Infrared Deep Sky Survey. The astrometry at the individual epochs was provided by the CASU as part of the standard UKIDSS pipeline. The catalogues were retrieved from the archive hosted by the Wide Field Astronomy Unit (WFAU) at the Institute for Astronomy, University of Edinburgh. The authors would like to acknowledge the Marie Curie 7th European Community Framework Programme grant n.247593 Interpretation and Parametrization of Extremely Red COOL dwarfs (IPERCOOL) International Research Staff Exchange Scheme. AHA acknowledges CNPq grant PQ306775/2009-3. This research has made use of the SIMBAD data base and VizieR catalogue access tool, operated at CDS, Strasbourg, France. This research has made use of NASA's Astrophysics Data System Bibliographic Services. This research has made use of SAOImage DS9, developed by Smithsonian Astrophysical Observatory.

REFERENCES

Abad C., Vieira K., Bongiovanni A., Romero L., Vicente B., 2003, A&A, 397, 345
Abell G. O., 1959, Astron. Soc. Pac. Leaflet, 8, 121
Andrei A. H. et al., 2009, A&A, 505, 385
Andrei A. H. et al., 2011, AJ, 141, 54
Bakos G. Á., Sahu K. C., Németh P., 2002, ApJ, 141, 187
Becklin E. E., Zuckerman B., 1988, Nature, 336, 656
Burgasser A. J., 2004, ApJ, 155, 191
Burgasser A. J., Geballe T. R., Leggett S. K., Kirkpatrick J. D., Golimowski D. A., 2006, ApJ, 637, 1067
Burgasser A. J. et al., 2011, ApJ, 735, 116
Burningham B. et al., 2010, MNRAS, 404, 1952
Burningham B. et al., 2011, MNRAS, 414, 3590
Burningham B. et al., 2013, MNRAS, 433, 457
Casali M. et al., 2001, in Clowes R., Adamson A., Bromage G., eds, ASP Conf. Ser. Vol. 232, The UKIRT IR Wide-Field Camera (WFCAM). Astron. Soc. Pac., San Francisco, p. 357
Casali M. et al., 2007, A&A, 467, 777
Casewell S. L., Jameson R. F., Burleigh M. R., 2008, MNRAS, 390, 1517
Catalán S. et al., 2012, A&A, 546, L3
Collins R., Hambly N., 2012, in Ballester P., Egret D., Lorente N. P. F., eds, ASP Conf. Ser. Vol. 461, Calculating Proper Motions in the WFCAM Science Archive for the UKIRT Infrared Deep Sky Surveys. Astron. Soc. Pac., San Francisco, p. 525

Cruz K. L., Reid I. N., Liebert J., Kirkpatrick J. D., Lowrance P. J., 2003, AJ, 126, 2421
Cruz K. L. et al., 2007, AJ, 133, 439
Day-Jones A. C. et al., 2011, MNRAS, 410, 705
Deacon N. R., Hambly N. C., Cooke J. A., 2005, A&A, 435, 363
Deacon N. R., Hambly N. C., King R. R., McCaughrean M. J., 2009, MNRAS, 394, 857
Deacon N. R. et al., 2012, ApJ, 755, 94
Dierickx M., Klement R., Rix H.-W., Liu C., 2010, ApJ, 725, L186
Dupuy T. J., Liu M. C., 2012, ApJ, 201, 19
Dye S. et al., 2006, MNRAS, 372, 1227
Epchtein N. et al., 1997, The Messenger, 87, 27
Faherty J. K., Burgasser A. J., Cruz K. L., Shara M. M., Walter F. M., Gelino C. R., 2009, AJ, 137, 1
Faherty J. K., Burgasser A. J., West A. A., Bochanski J. J., Cruz K. L., Shara M. M., Walter F. M., 2010, AJ, 139, 176
Feast M., Whitelock P., 1997, MNRAS, 291, 683
Finlator K. et al., 2000, AJ, 120, 2615
Goldman B., Marsat S., Henning T., Clemens C., Greiner J., 2010, MNRAS, 405, 1140
Gomes J. I. et al., 2013, MNRAS, 431, 2745
Greenstein J. L., 1980, ApJ, 242, 738
Hambly N. C. et al., 2008, MNRAS, 384, 637
Hansen B. M. S. et al., 1999, ApJ, 520, 680
Hawley S. L. et al., 2002, AJ, 123, 3409
Hewett P. C., Warren S. J., Leggett S. K., Hodgkin S. T., 2006, MNRAS, 367, 454
Høg E. et al., 2000, A&A, 355, L27
Kharchenko N. V., 2001, Kinematika Fiz. Nebesnykh Tel, 17, 409
Kilic M., Munn J. A., Harris H. C., Liebert J., von Hippel T., Williams K. A., Metcalfe T. S., Winget D. E., 2005, in Koester D., Moehler S., eds, ASP Conf. Ser. Vol. 334, Discovery of 282 Cool White Dwarfs ($T_{\rm eff}$ 8000 K) in the Sloan Digital Sky Survey. Astron. Soc. Pac., San Francisco, p. 131
Kilic M., Burrows A., Kuchner M., Reach W., Winget D., von Hippel T., 2006, in Spitzer Proposal ID #30208, Resolving Mysteries: Ultra-Cool White Dwarfs and the Age of the Galaxy.
Kilic M. et al., 2010, ApJ, 190, 77
Kirkpatrick J. D., 2000, in Griffith C. A., Marley M. S., eds, ASP Conf. Ser. Vol. 212, The L and T Dwarf Spectral Sequences: First Steps in Bridging the Gap Between Planets and Stars. Astron. Soc. Pac., San Francisco, p. 20
Kirkpatrick J. D., 2011, in Johns-Krull C., Browning M. K., West A. A., eds, ASP Conf. Ser. Vol. 448, New Surveys for Brown Dwarfs and Their Impact on the IMF. Astron. Soc. Pac., San Francisco, p. 323
Kirkpatrick J. D. et al., 1999, ApJ, 519, 802
Kirkpatrick J. D. et al., 2008, ApJ, 689, 1295
Kirkpatrick J. D. et al., 2010, ApJ, 190, 100
Kirkpatrick J. D., Cushing M. C., Gelino C. R., Griffith R. L., Skrutskie M. F., Marsh K. A., Wright E., 2011, ApJ, 197, 19
Kirkpatrick J. D. et al., 2012, ApJ, 753, 156
Knapp G. R. et al., 2004, AJ, 127, 3553
Latham D. W., Stefanik R. P., Torres G., Davis R. J., Mazeh T., Carney B. W., Laird J. B., Morse J. A., 2002, AJ, 124, 1144
Lawrence A., Warren S. J., Almaini O., Edge A. C., Hambly N. C., Jameson R. F., Lucas P., Casali E., 2007, MNRAS, 379, 1599
Leggett S. K. et al., 2009, ApJ, 695, 1517
Leggett S. K. et al., 2010, ApJ, 710, 1627
Leggett S. K., Lodieu N., Tremblay P.-E., Bergeron P., Nitta A., 2011, ApJ, 735, 62
Leggett S. K. et al., 2012, ApJ, 748, 74
Lépine S., Shara M. M., 2005, AJ, 129, 1483
Lépine S., Shara M. M., Rich R. M., 2002, AJ, 124, 1190
Looper D. L., Kirkpatrick J. D., Burgasser A. J., 2007, AJ, 134, 1162
Luyten W. J., 1979a, LHS Catalogue. A Catalogue of Stars with Proper Motions Exceeding 0”5 Annually, 2nd edn. University of Minnesota, Minneapolis
Luyten W. J., 1979b, NLTT Catalogue. Volume_I. +90__to_+30_. Volume._II. +30__to_0_. Univ. Minnesota, Minneapolis
Marocco F. et al., 2010, A&A, 524, A38
Mason B. D., Wycoff G. L., Hartkopf W. I., Douglass G. G., Worley C. E., 2001, AJ, 122, 3466
Meng X.-C., Yang W.-M., Li Z.-M., 2010, Res. Astron. Astrophys., 10, 927
Munn J. A. et al., 2004, AJ, 127, 3034
Murray D. N. et al., 2011, MNRAS, 414, 575
Pinfield D. J., Jones H. R. A., Lucas P. W., Kendall T. R., Folkes S. L., Day-Jones A. C., Chappelle R. J., Steele I. A., 2006, MNRAS, 368, 1281
Pinfield D. J., Burningham B., Tamura M., Leggett S. K., Lodieu N., Lucas P. W., Mortlock D. J., Warren E., 2008, MNRAS, 390, 304
Pinfield D. J. et al., 2012, MNRAS, 422, 1922
Reid I. N., 2003, AJ, 126, 2449
Reid I. N., Gizis J. E., 2005, PASP, 117, 676
Reid I. N. et al., 1991, PASP, 103, 661
Roeser S., Demleitner M., Schilbach E., 2010, AJ, 139, 2440
Salim S., Gould A., 2003, ApJ, 582, 1011
Sayres C., Subasavage J. P., Bergeron P., Dufour P., Davenport J. R. A., AlSayyad Y., Tofflemire B. M., 2012, AJ, 143, 103
Schilbach E., Röser S., Scholz R.-D., 2009, A&A, 493, L27
Scholz R.-D., 2010, A&A, 515, A92
Sheppard S. S., Cushing M. C., 2009, AJ, 137, 304
Skrutskie M. F., Cutri R. M., Stiening R., Weinberg M. D., Schneider S., Carpenter J. M., Beichman C. E., 2006, AJ, 131, 1163
Smith L., Lucas P., Burningham B., Jones H., Smart R., Pinfield D., Marocco F., Clarke J., 2013, preprint (arXiv:1303.5288)
Taylor M. B., 2005, in Shopbell P., Britton M., Ebert R., eds, ASP Conf. Ser. Vol. 347, TOPCAT & STIL: Starlink Table/VOTable Processing Software. Astron. Soc. Pac., San Francisco, p. 29
Taylor M. B., 2006, in Gabriel C., Arviset C., Ponz D., Enrique S., eds, ASP Conf. Ser. Vol. 351, STILTS – A Package for Command-Line Processing of Tabular Data. Astron. Soc. Pac., San Francisco, p. 666
Vick A., Folger M., McLay S., Pickup A., 2004, in Ochsenbein F., Allen M. G., Egret D., eds, ASP Conf. Ser. Vol. 314, The WFCAM Instrument Software. Astron. Soc. Pac., San Francisco, p. 732
Warren S., 2002, in Tyson J. A., Wolff S., eds, SPIE Conf. Ser. Vol. 4836, Scientific Goals of the UKIRT Infrared Deep Sky Survey. SPIE, Bellingham, p. 313
West A. A., Hawley S. L., Bochanski J. J., Covey K. R., Reid I. N., Dhital S., Hilton E. J., Masuda M., 2008, AJ, 135, 785
West A. A. et al., 2011, AJ, 141, 97
Zhang Z. H. et al., 2009, A&A, 497, 619
Zhang Z. H. et al., 2010, MNRAS, 404, 1817

APPENDIX A: CATALOGUE SAMPLE

Table A1 gives a sample of 10 rows from the catalogue, the column headers correspond to the following.

Line – links the same line across the splits in this sample table.
RA – right ascension of first epoch *J* band detection.
Dec. – declination of first epoch *J* band detection.
Y – UKIDSS DR10 Y magnitude.
e_Y – uncertainty on UKIDSS DR10 Y magnitude.
J1 – UKIDSS FITS File first epoch *J* band magnitude.
e_J1 – uncertainty on UKIDSS FITS File first epoch *J* band magnitude.
J2 – UKIDSS FITS File second epoch *J* band magnitude.
e_J2 – uncertainty on UKIDSS FITS File second epoch *J* band magnitude.
H – UKIDSS DR10 H magnitude.
e_H – uncertainty on UKIDSS DR10 H magnitude.
K – UKIDSS DR10 K magnitude.
e_K – uncertainty on UKIDSS DR10 K magnitude.

Table A1. Catalogue sample.

Line	RA	Dec.	Y	e_Y	J1	e_J1	J2	e_J2	H	e_H
1	0.00606	−0.673361	15.473	0.0050	14.969	0.01	14.987	0.01	14.43	0.0050
2	0.012379	−0.605281	−9.9999949E8	−9.9999949E8	19.708	0.219	19.429	0.179	18.809	0.195
3	0.016784	−0.799593	−9.9999949E8	−9.9999949E8	19.2	0.142	19.294	0.159	−9.9999949E8	−9.9999949E8
4	0.025975	−0.702338	13.481	0.0020	13.081	0.01	13.088	0.01	12.545	0.0020
5	0.028177	−1.142162	16.55	0.0090	16.095	0.01	16.116	0.01	15.497	0.01
6	0.062918	15.916086	14.303	0.0030	13.892	0.01	13.785	0.01	13.156	0.0020
7	0.070539	15.928027	15.103	0.0040	14.555	0.01	14.591	0.01	14.074	0.0040
8	0.102226	15.828653	16.047	0.0070	15.565	0.014	15.561	0.01	15.067	0.0090
9	0.108392	15.845481	19.093	0.082	18.358	0.153	18.559	0.077	18.3	0.152
10	0.1466	15.906866	18.214	0.038	18.086	0.122	17.719	0.037	17.216	0.057

Line	K	e_K	J1ell	J1PA	J2ell	J2PA	J1class	J2class	RAPM_rel	DecPM_rel	e_RAPM_rel
1	14.162	0.0060	0.08	−72.6	0.08	−26.81	−1	−1	−15.44	−21.9	3.98
2	−9.9999949E8	−9.9999949E8	0.4	63.01	0.24	61.0	1	−1	44.66	−112.37	12.0
3	−9.9999949E8	−9.9999949E8	0.41	−17.6	0.25	−88.07	−7	−1	175.51	164.84	13.45
4	12.329	0.0020	0.05	−78.73	0.06	−17.92	−1	−1	−78.6	−52.84	6.89
5	15.258	0.014	0.03	151.43	0.08	153.55	−1	−1	43.49	−22.88	6.94
6	12.906	0.0030	0.34	106.41	0.06	122.9	1	−1	−158.3	39.32	7.94
7	13.827	0.0050	0.02	77.86	0.04	126.85	−1	−1	81.27	32.61	7.81
8	14.778	0.011	0.03	70.5	0.04	108.77	−1	−1	−63.07	−30.77	6.96
9	17.535	0.123	0.12	127.78	0.42	124.2	−1	1	115.6	−68.38	15.74
10	17.106	0.084	0.33	42.7	0.06	160.08	−7	−1	67.12	−55.98	11.44

Line	e_DecPM_rel	RAPM	DecPM	e_RAPM	e_DecPM	J1MJDobs	EpochBaseline	SourceID	local
1	4.89	−22.33	−27.04	3.98	4.89	53634.42578	6.069462286	433867580351	true
2	11.59	37.78	−117.51	12.0	11.59	53634.42578	6.069462286	433867580667	false
3	13.14	168.63	159.7	13.45	13.14	53634.42578	6.069462286	433867580597	false
4	4.06	−85.49	−57.98	6.89	4.06	53634.42578	6.069462286	433867580292	true
5	5.85	36.72	−28.0	6.94	5.85	53634.42578	6.069462286	433870019429	true
6	7.03	−163.67	31.52	7.94	7.03	54398.37891	3.999807474	433804633469	true
7	5.89	75.9	24.81	7.81	5.89	54398.37891	3.999807474	433804633507	true
8	7.26	−68.44	−38.57	6.96	7.26	54398.37891	3.999807474	433804633203	true
9	15.89	110.23	−76.18	15.74	15.89	54398.37891	3.999807474	433804633253	true
10	11.87	61.75	−63.78	11.44	11.87	54398.37891	3.999807474	433804633434	false

J1ell – ellipticity of first epoch *J* band detection.

J1PA – position angle of ellipticity of first epoch *J* band detection.

J2ell – ellipticity of second epoch *J* band detection.

J2PA – position angle of ellipticity of second epoch *J* band detection.

J1class – morphological classification of first epoch *J* band detection.

J2class – morphological classification of second epoch *J* band detection.

RAPM_rel – relative proper motion in Right ascension ($\times \cos\delta$).

DecPM_rel – relative proper motion in declination.

e_RAPM_rel – uncertainty on relative proper motion in right ascension ($\times \cos\delta$).

e_DecPM_rel – uncertainty on relative proper motion in declination.

RAPM – proper motion in right ascension ($\times \cos\delta$).

DecPM – proper motion in declination.

e_RAPM – uncertainty on proper motion in right ascension ($\times \cos\delta$).

e_DecPM – uncertainty on proper motion in declination.

J1MJDobs – modified Julian date of first epoch observation.

EpochBaseline – epoch baseline in decimal years.

SourceID – UKIDSS DR10 sourceID (for WSA cross-matching).

local – local/global transformation flag ('true' indicates a local transform was used).

Right ascension, declination and position angles are in units of decimal degrees. All UKIDSS magnitudes are AperMag3 values (2 arcsec aperture), with −9.999E8 as the null value. Proper motions and uncertainties are in units of mas yr^{-1}. Morphological classification flags are as follows:

1 – galaxy
0 – Noise
−1 – Star
−2 – Probable star
−7 – Bad pixel within 2 arcsec aperture
−9 – Saturated.

The CASU standard source extraction documentation contains more information on these morphological classifications.

SUPPORTING INFORMATION

Additional Supporting Information may be found in the online version of this article:

Table A1. Catalogue sample (http://mnras.oxfordjournals.org/lookup/suppl/doi:10.1093/mnras/stt2156/-/DC1).

Please note: Oxford University Press is not responsible for the content or functionality of any supporting materials supplied by the authors. Any queries (other than missing material) should be directed to the corresponding author for the article.

This paper has been typeset from a TEX/LATEX file prepared by the author.